

16. SITE 1022¹

Shipboard Scientific Party²

HOLE 1022A

Date occupied: 11 June 1996
Date departed: 12 June 1996
Time on hole: 19 hr
Position: 40°4.850'N, 125°20.559'W
Drill pipe measurement from rig floor to seafloor (m): 1938.4
Distance between rig floor and sea level (m): 11.4
Water depth (drill pipe measurement from sea level, m): 1927.0
Total depth (from rig floor, m): 2104.4
Penetration (m): 166.0
Number of cores (including cores having no recovery): 18
Total length of cored section (m): 166.0
Total core recovered (m): 171.6
Core recovery (%): 103.0
Oldest sediment cored:
Depth (mbsf): 166.0
Nature: Nannofossil with clay and diatoms, diatom nannofossil ooze with clay, clay with diatoms
Age: early Pliocene
Measured velocity (km/s): 1.546 at interval 6H-6, 82–85 cm

HOLE 1022B

Date occupied: 12 June 1996
Date departed: 12 June 1996
Time on hole: 10 hr, 15 min
Position: 40°4.850'N, 125°20.561'W
Drill pipe measurement from rig floor to seafloor (m): 1937.3
Distance between rig floor and sea level (m): 11.4
Water depth (drill pipe measurement from sea level, m): 1925.9
Total depth (from rig floor, m): 2038.5
Penetration (m): 101.2
Number of cores (including cores having no recovery): 11
Total length of cored section (m): 101.2
Total core recovered (m): 105.7
Core recovery (%): 104.0
Oldest sediment cored:
Depth (mbsf): 101.2

Nature: Nannofossil clay mixed sediment with diatoms, clayey nannofossil ooze with diatoms
Age: late Pliocene

HOLE 1022C

Date occupied: 12 June 1996
Date departed: 15 June 1996
Time on hole: 2 days, 23 hr, 15 min
Position: 40°4.842'N, 125°20.558'W
Drill pipe measurement from rig floor to seafloor (m): 1937.5
Distance between rig floor and sea level (m): 11.4
Water depth (drill pipe measurement from sea level, m): 1926.1
Total depth (from rig floor, m): 2325.2
Penetration (m): 387.7
Number of cores (including cores having no recovery): 42
Total length of cored section (m): 387.7
Total core recovered (m): 378.85
Core recovery (%): 97.7
Oldest sediment cored:
Depth (mbsf): 387.7
Nature: Porcellanite
Age: early Pliocene–late Miocene(?)

Principal results: Site 1022 is situated on the continental slope just south of the Mendocino Fracture Zone about 90 km from Cape Mendocino. The drill site is located at a water depth of 1926 mbsl on a sliver of continental crust that may have been transferred to the Pacific Plate in the Oligocene. The main objective for drilling at Site 1022 was to obtain a record of surface and deep-water properties from the Miocene through the Quaternary. Because this site is located only 90 km from the coast, the sediments should provide a good record of coastal upwelling and organic matter diagenesis. Geochemical indices of paleoproductivity and microfossil assemblages obtained from Site 1022 will also provide important data on nutrients carried by the California Current and upon how the carbon cycle can be affected by changes in productivity and climate.

Three holes were cored with the APC/XCB at Site 1022 (Fig. 1) to a maximum depth of 387.8 mbsf, recovering an interval of Quaternary to late Miocene(?)–early Pliocene (0.0–6.0[?] Ma) age. Hole 1022A was cored with the APC to 166.0 mbsf. Hole 1022B was cored with the APC to 101.2 mbsf. Hole 1022C was cored with the APC to 159.5 mbsf and deepened with the XCB to 387.7 mbsf. The hole was logged with the density-porosity combination tool string, the combined sonic-Formation MicroScanner, and the GHMT tool strings. Detailed comparisons between the magnetic susceptibility and the GRAPE density record generated on the MST, and high-resolution color reflectance measured with the Oregon State University system, demonstrated complete recovery of the sedimentary sequence down to 170 mcd.

The sedimentary sequence is divided into three parts: an upper nannofossil-dominated interval, a middle siliciclastic clay-dominated interval, and a lower biosiliceous interval. These lithostratigraphic units are further

¹Lyle, M., Koizumi, I., Richter, C., et al., 1997. *Proc. ODP, Init. Repts.*, 167: College Station, TX (Ocean Drilling Program).

²Shipboard Scientific Party is given in the list preceding the Table of Contents.

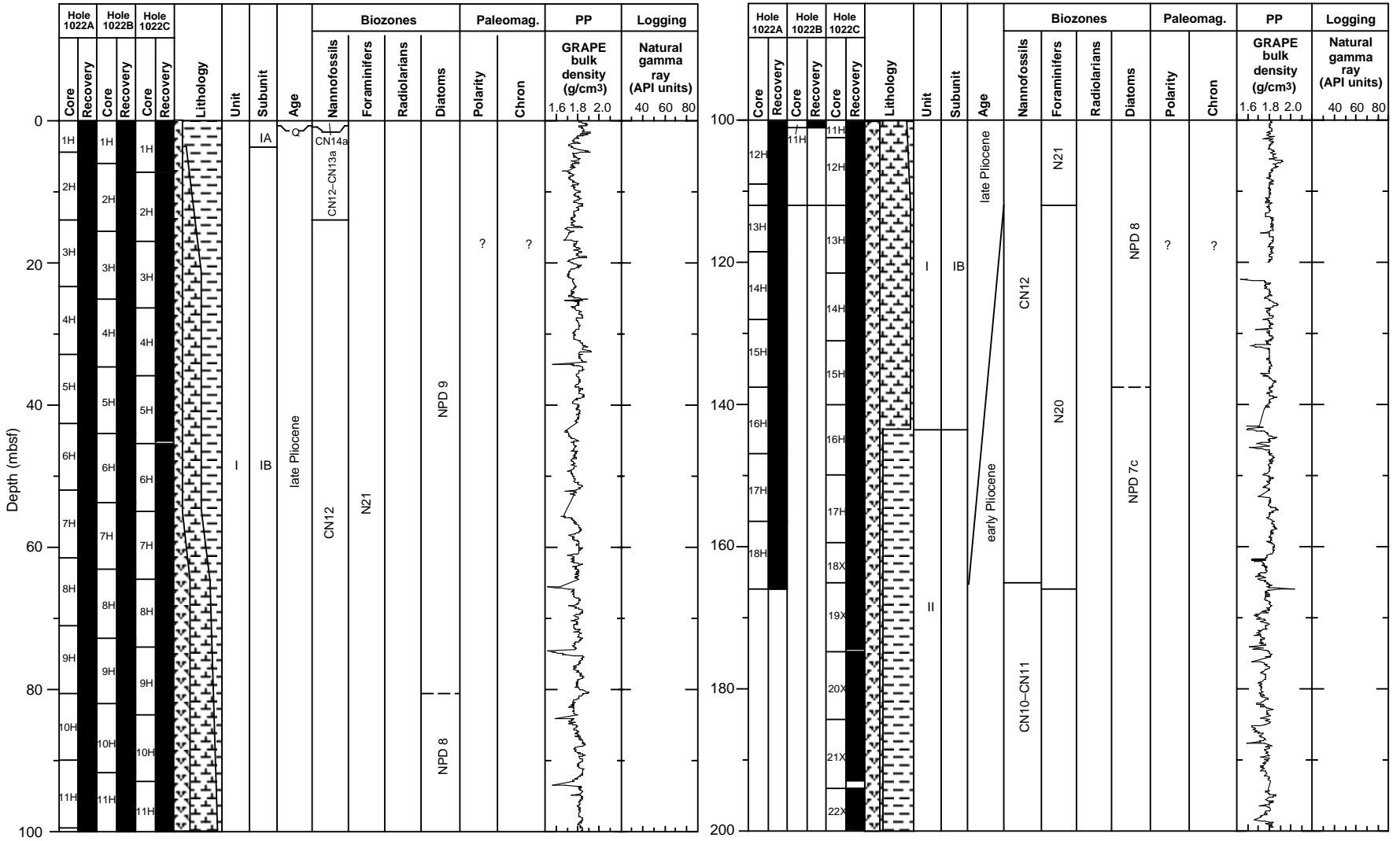


Figure 1. Site 1022 master column.

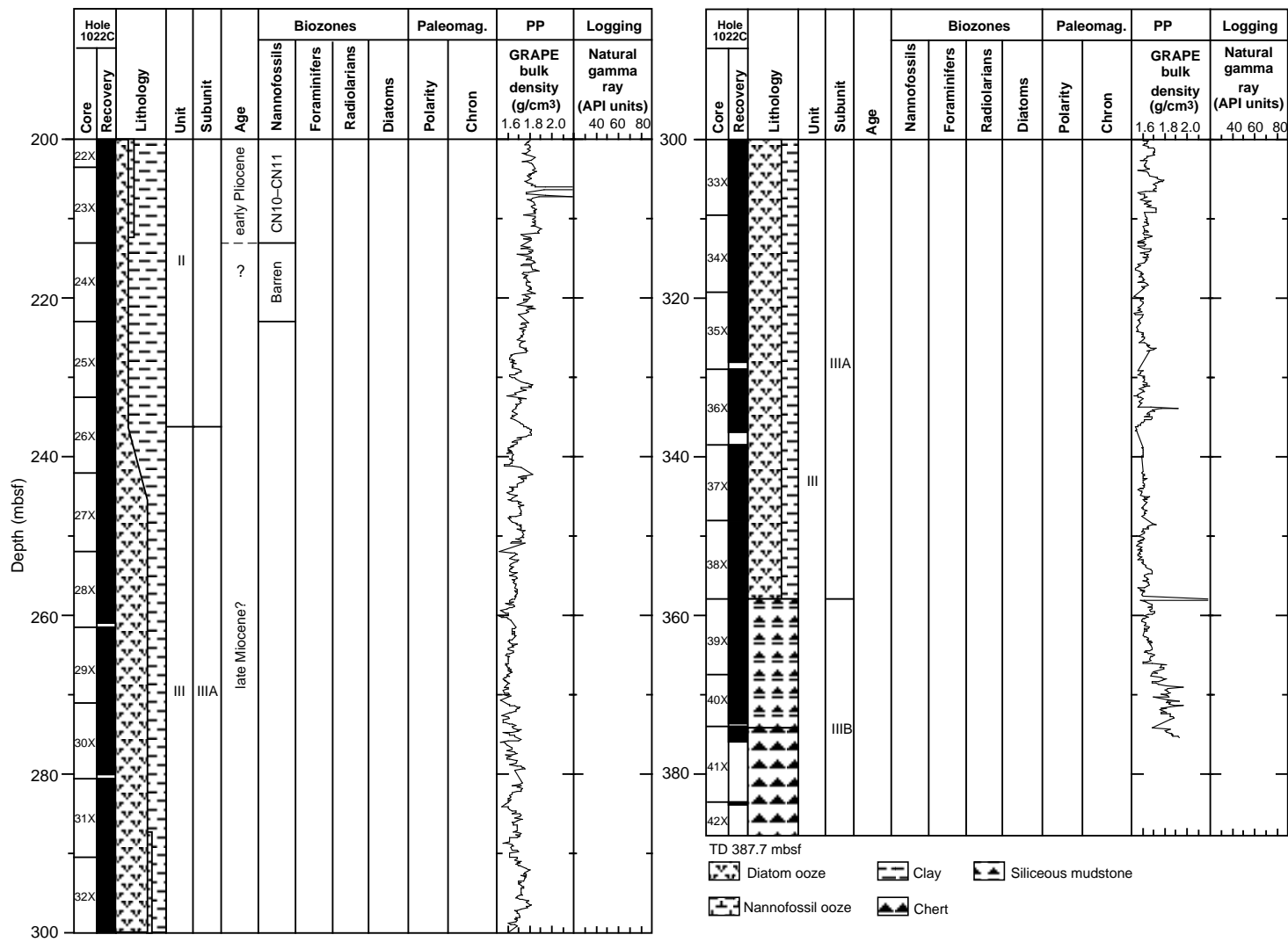


Figure 1 (continued).

divided into subunits based on minor changes in composition or diagenesis. The uppermost part of the sequence is marked by a 1- to 3-m-thick bed of glauconitic clay with silt and diatoms, which represents the entire Quaternary. Below this layer, the upper part of the sequence is dominated by nannofossil clay to nannofossil ooze and diatom clay. This unit includes minor volcanic ash and barite-cemented horizons. The middle part of the sequence is dominated by clay to diatom clay with infrequent interbeds of clayey nannofossil ooze. Diatom content increases from the middle part to the lower unit, which consists of diatomite and clayey diatomite. A diagenetic boundary occurs at 360 mbsf where diatomite is transformed into interbedded siliceous mudstone and chert. Infrequent, decimeter-thick dolostone beds occur in all parts of the sequence.

Shipboard biostratigraphy, organic geochemistry, and inorganic geochemistry, were essentially limited to Hole 1022A because of time constraints at the end of Leg 167. Only reconnaissance information is now available for the deeper interval in Hole 1022C. Hole 1022A consists of 166 m of upper Pliocene through possible uppermost lower Pliocene sediments. The Quaternary is represented only by a very thin (<1 m) veneer of sediments overlying the late Pliocene. The total age range of the sedimentary sequence recovered from Holes 1022A and 1022B is not well constrained. Planktonic foraminifers indicate that the top of the sequence is >2.25 Ma and that the base of Hole 1022A is older than 3.3 Ma. Calcareous nannofossils indicate that the age of the base of Hole 1022A is <3.8 Ma. Because the sedimentation rate is high, each of the four groups examined is represented by only one or two biozones, and few datums are recognized.

All of the microfossil groups in Holes 1022A and 1022B are represented by cool, relatively high-latitude assemblages. Radiolarians are entirely represented by subarctic forms. Diatoms are dominated by North Pacific subarctic assemblages. Planktonic foraminifer assemblages are dominated by subarctic to cool temperate forms, with subtropical elements absent.

Both diatoms and radiolarians show evidence of strong upwelling throughout the Pliocene. The upper Pliocene sequence at Site 1022 is the most diatomaceous of all Leg 167 sites. Radiolarians indicate a prevalence of strong coastal upwelling, while the diatoms reflect oscillations between strong coastal upwelling and oceanic upwelling. Benthic foraminifers throughout are typical middle bathyal deep sea assemblages indicative of well-oxygenated bottom waters.

Low magnetic intensities and a drilling-induced overprint precluded the establishment of a magnetic chronostratigraphy.

Volatile hydrocarbon concentrations were very high. Gases up to C₆ occurred at about 100 mbsf in the sediment, probably derived by thermogenic degradation of organic material. Although methane/ethane ratios decrease with depth, no indication of migrated hydrocarbons was observed. Calcium carbonate values increased within the upper 100 mbsf to a maximum of about 30 wt% and decreased again to minima near 5 wt% at the bottom of Hole 1022A. Organic carbon concentrations varied between 0.5 and 1.5 wt%, showing slightly increased values in lithostratigraphic Unit II. The organic matter is mainly of marine origin.

Chemical gradients in the interstitial waters reflect organic matter diagenesis, the dissolution of biogenic opal and calcium carbonate, the influence of authigenic mineral precipitation reactions, and the diffusive influence of reactions in underlying basalt.

Downhole temperature measurements yield a thermal gradient of 88°C/km. Using an average measured thermal conductivity of 0.950 W/(m·K) provides a heat-flow estimate of 84 mW/m² at Site 1022.

BACKGROUND AND OBJECTIVES

General Description

Site 1022, on the continental slope just south of the Mendocino Fracture Zone ~90 km from Cape Mendocino, is located at a depth of 1926 mbsl on a sliver of continental crust apparently carried seaward along the Mendocino Fracture Zone (Fig. 2). It is unknown how far Site 1022 has moved along the coast but it could have originated as

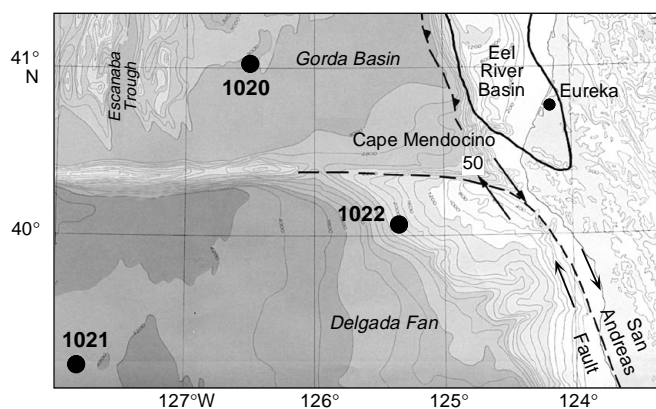


Figure 2. Location map for Site 1022. It is located on a continental fragment, based on DSDP Site 173 drilling, transported seaward along the Mendocino Fracture Zone just to the north.

far south as the California Borderland in the Oligocene. Site 1022 is located about 16 km from DSDP Site 173, which drilled into an andesitic basement of late Oligocene age (Ingle, 1973). The sediment column recovered at Site 1022 consists of a thin veneer (<1 m) of Quaternary sediments overlying upper Pliocene-upper Miocene(?) sediments, although the age of the lowermost interval is poorly constrained.

The site, surveyed in detail on the *Maurice Ewing* cruise EW9504 in 1995 and in 1994 on *Wecoma* cruise W9406 (Lyle et al., 1995a, 1995b; Fig. 3), is located a few kilometers north of a submarine canyon on a gentle slope. A relatively thick sediment column of 695 ms TWT (about 560 m) lies above acoustic basement. The upper part of the sediment column is well layered, and a prominent reflector similar to chert reflectors at other Leg 167 drill sites appears ~420 ms TWT below the seafloor (about 330 mbsf).

Site Objectives

Site 1022 is slightly shallower than Site 1018 (Guide Seamount) and was drilled to construct water column depth profiles, especially for studies of calcium carbonate preservation and to obtain records of surface and deep-water properties. Since it is located only 90 km from the coast, the sediments have been strongly influenced by coastal upwelling. It is the companion to Sites 1020 and 1021 for comparison of inshore conditions to those within the California Current proper.

Site 1022 had important geochemical objectives. Organic carbon content varied around 1% with an intermediate geothermal gradient. This environment provides one of the end-members needed to study preservation of bulk organic matter and of specific organic molecules. Geochemical indices of paleoproductivity and microfossil assemblages obtained from Site 1022 will also provide important data on nutrients carried by the California Current and upon how the carbon cycle can be affected by changes in productivity and climate.

OPERATIONS

Transit from Site 1021 to Site 1022

The 128.0-nmi transit from Site 1021 to Site 1022 was accomplished in 13.5 hr at an average speed of 9.5 kt. The *JOIDES Resolution* arrived at Site 1022 at 0500 hr on 11 June.

Hole 1022A

Hole 1022A was spudded at 1015 hr on 11 June. APC Cores 167-1022A-1H through 18H were taken down to 166.0 mbsf with 103.4% recovery (Table 1; see Table 2 on CD-ROM in the back pocket of this

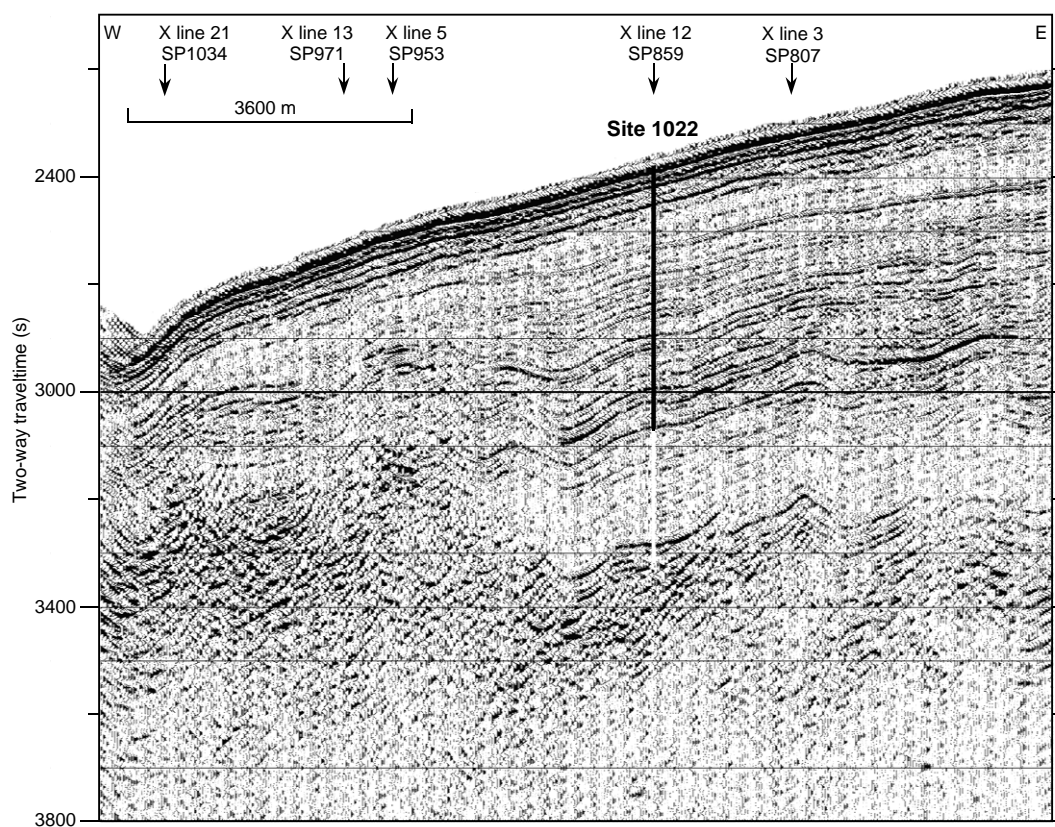


Figure 3. An east-west seismic reflection profile through Site 1022 (Line EW9504 CA2-23; Lyle et al., 1995a, 1995b). The summed 4-channel data were filtered between 30 and 200 Hz, with predictive deconvolution and Stolt F-K migration applied. On y-axis, (s) = milliseconds.

volume for a more detailed coring summary). Adara temperature measurements were taken on Cores 167-1022A-4H, 6H, and 8H (see “Physical Properties” section, this chapter). Oriented cores were obtained starting with Core 167-1022A-3H.

Hole 1022B

The vessel was offset 10 m to the south and Hole 1022B was spudded at 0215 hr on 12 June. APC Cores 167-1022B-1H through 11H were taken down to 101.2 mbsf with 105.7% recovery (Table 1).

Hole 1022C

The vessel was offset 10 m to the south and Hole 1022C was spudded at 1115 hr on 12 June. APC Cores 167-1022C-1H through 17H were taken to 159.5 mbsf with 103.3% recovery. XCB Cores 167-1022C-18X through 42X were taken down to 387.7 mbsf with 93.9% recovery (Table 1). Hole 1022C was logged with the density-positivity, combined sonic-Formation MicroScanner, and GHMT tool strings with excellent results. The drill string was tripped back to the surface and secured for the 18-hr transit to San Francisco by 0930 hr on 15 June.

LITHOSTRATIGRAPHY

Introduction

A Quaternary to late Miocene-early Pliocene sequence was cored at Site 1022. The sequence is divided into three lithostratigraphic units on the basis of visual core description, smear-slide analysis, and X-ray diffraction: an upper nannofossil and clay interval (Unit I), a middle siliciclastic clay-dominated interval (Unit II), and a lower bisiliceous interval (Unit III). These units are further divided into sub-

units based on minor changes in composition or diagenesis (Fig. 4). The uppermost part of the sequence (Subunit IA) is marked by a 1- to 3-m-thick bed of glauconitic clay with silt, pyrite, and diatoms that represents the entire Quaternary. Below this layer, the upper part of the sequence (Subunit IB) is dominated by nannofossil clay to nannofossil ooze, associated with decreasing quantities of clay and minor diatoms. Volcanic ash and barite-cemented horizons are also present in this unit. Unit II is dominated by clay to diatom clay with infrequent interbeds of clayey nannofossil ooze. Diatom content gradually increases in the transition to Subunit IIIA, which is dominated by diatomite and clayey diatomite. A diagenetic boundary was encountered at ~360 mbsf, where diatomite is underlain by siliceous mudstone interbedded with decimeter-thick chert layers (Subunit IIIB). Infrequent, decimeter-thick dolostone beds occur in all parts of the sequence. Cores were described extremely rapidly at this site, the last of Leg 167. Consequently, the detail and accuracy of sedimentologic analysis may not equal the exalted levels reached at the previous Leg 167 sites.

Description of Units

Unit I

Hole 1022A, interval 167-1022A-1H-1 through 15H-CC; 0–137.5 mbsf;
 Hole 1022B, interval 167-1022B-1H-1 through 11H-CC; 0–101.2 mbsf
 (bottom of hole);
 Hole 1022C, interval 167-1022C-1H-1 through 15H-CC; 0–140.5 mbsf.
 Age: Quaternary to late Pliocene, 0.0(?) to ~3.58 Ma.

Unit I is chiefly composed of nannofossils and siliciclastic clay with minor diatoms. These components produce thick, irregular alternations of nannofossil ooze to nannofossil clay, clay with silt and di-

Table 1. Coring summary for Site 1022.

Core	Date (June 1996)	Time	Top (mbsf)	Bottom (mbsf)	Length cored (m)	Length recovered (m)	Recovery (%)	Comments
167-1022A-								
1H	11	1730	0.0	4.5	4.5	4.55	101.0	
2H	11	1815	4.5	14.0	9.5	10.07	106.0	
3H	11	1900	14.0	23.5	9.5	10.04	105.7	
4H	11	1950	23.5	33.0	9.5	9.93	104.0	
5H	11	2025	33.0	42.5	9.5	9.95	105.0	
6H	11	2120	42.5	52.0	9.5	9.83	103.0	
7H	11	2155	52.0	61.5	9.5	9.85	103.0	
8H	11	2245	61.5	71.0	9.5	10.24	107.8	
9H	11	2325	71.0	80.5	9.5	10.01	105.3	
10H	12	0000	80.5	90.0	9.5	10.06	105.9	
11H	12	0040	90.0	99.5	9.5	9.79	103.0	
12H	12	0120	99.5	109.0	9.5	9.89	104.0	
13H	12	0200	109.0	118.5	9.5	10.19	107.2	
14H	12	0235	118.5	128.0	9.5	10.18	107.1	
15H	12	0320	128.0	137.5	9.5	10.01	105.3	
16H	12	0410	137.5	147.0	9.5	10.02	105.5	
17H	12	0455	147.0	156.5	9.5	10.15	106.8	First 7K core!
18H	12	0530	156.5	166.0	9.5	6.81	71.7	
167-1022B-								
1H	12	0925	0.0	6.2	6.2	6.14	99.0	
2H	12	1010	6.2	15.7	9.5	10.04	105.7	
3H	12	1045	15.7	25.2	9.5	9.90	104.0	
4H	12	1125	25.2	34.7	9.5	10.15	106.8	
5H	12	1205	34.7	44.2	9.5	10.01	105.3	
6H	12	1300	44.2	53.7	9.5	9.94	104.0	
7H	12	1340	53.7	63.2	9.5	9.97	105.0	
8H	12	1420	63.2	72.7	9.5	9.90	104.0	
9H	12	1500	72.7	82.2	9.5	9.62	101.0	
10H	12	1545	82.2	91.7	9.5	9.89	104.0	
11H	12	1600	91.7	101.2	9.5	10.13	106.6	
167-1022C-								
1H	12	1830	0.0	7.5	7.5	7.45	99.3	
2H	12	1910	7.5	17.0	9.5	9.68	102.0	
3H	12	1940	17.0	26.5	9.5	9.87	104.0	
4H	12	2005	26.5	36.0	9.5	9.68	102.0	
5H	12	2035	36.0	45.5	9.5	9.19	96.7	
6H	12	2100	45.5	55.0	9.5	10.05	105.8	
7H	12	2130	55.0	64.5	9.5	9.84	103.0	
8H	12	2205	64.5	74.0	9.5	9.52	100.0	
9H	12	2230	74.0	83.5	9.5	9.71	102.0	
10H	12	2300	83.5	93.0	9.5	9.98	105.0	
11H	12	2340	93.0	102.5	9.5	9.68	102.0	
12H	13	0020	102.5	112.0	9.5	10.05	105.8	
13H	13	0055	112.0	121.5	9.5	9.63	101.0	
14H	13	0130	121.5	131.0	9.5	10.24	107.8	
15H	13	0200	131.0	140.5	9.5	9.83	103.0	
16H	13	0230	140.5	150.0	9.5	10.19	107.2	
17H	13	0300	150.0	159.5	9.5	10.10	106.3	
18X	13	0440	159.5	165.2	5.7	6.18	108.0	
19X	13	0535	165.2	174.8	9.6	9.45	98.4	
20X	13	0640	174.8	184.4	9.6	9.96	104.0	
21X	13	0800	184.4	194.0	9.6	8.77	91.3	
22X	13	0920	194.0	203.6	9.6	9.55	99.5	
23X	13	1045	203.6	213.2	9.6	9.56	99.6	
24X	13	1235	213.2	222.9	9.7	9.74	100.0	
25X	13	1330	222.9	232.5	9.6	9.94	103.0	
26X	13	1500	232.5	242.1	9.6	9.89	103.0	
27X	13	1615	242.1	251.8	9.7	9.64	99.4	
28X	13	1730	251.8	261.4	9.6	9.23	96.1	
29X	13	1850	261.4	271.0	9.6	9.89	103.0	
30X	13	1955	271.0	280.6	9.6	8.90	92.7	
31X	13	2120	280.6	290.3	9.7	9.75	100.0	
32X	13	2225	290.3	299.9	9.6	9.87	103.0	
33X	13	2330	299.9	309.6	9.7	9.82	101.0	
34X	14	0030	309.6	319.3	9.7	9.62	99.2	
35X	14	0130	319.3	328.9	9.6	8.88	92.5	
36X	14	0310	328.9	338.6	9.7	8.14	83.9	
37X	14	0440	338.6	348.2	9.6	9.40	97.9	
38X	14	0530	348.2	357.8	9.6	9.79	102.0	
39X	14	0650	357.8	367.4	9.6	9.87	103.0	
40X	14	0900	367.4	374.0	6.6	6.13	92.9	
41X	14	1145	374.0	383.5	9.5	1.89	19.9	
42X	14	1350	383.5	387.7	4.2	0.30	7.1	

Note: Table 2, on the CD-ROM, back pocket, this volume, is a more detailed coring summary.

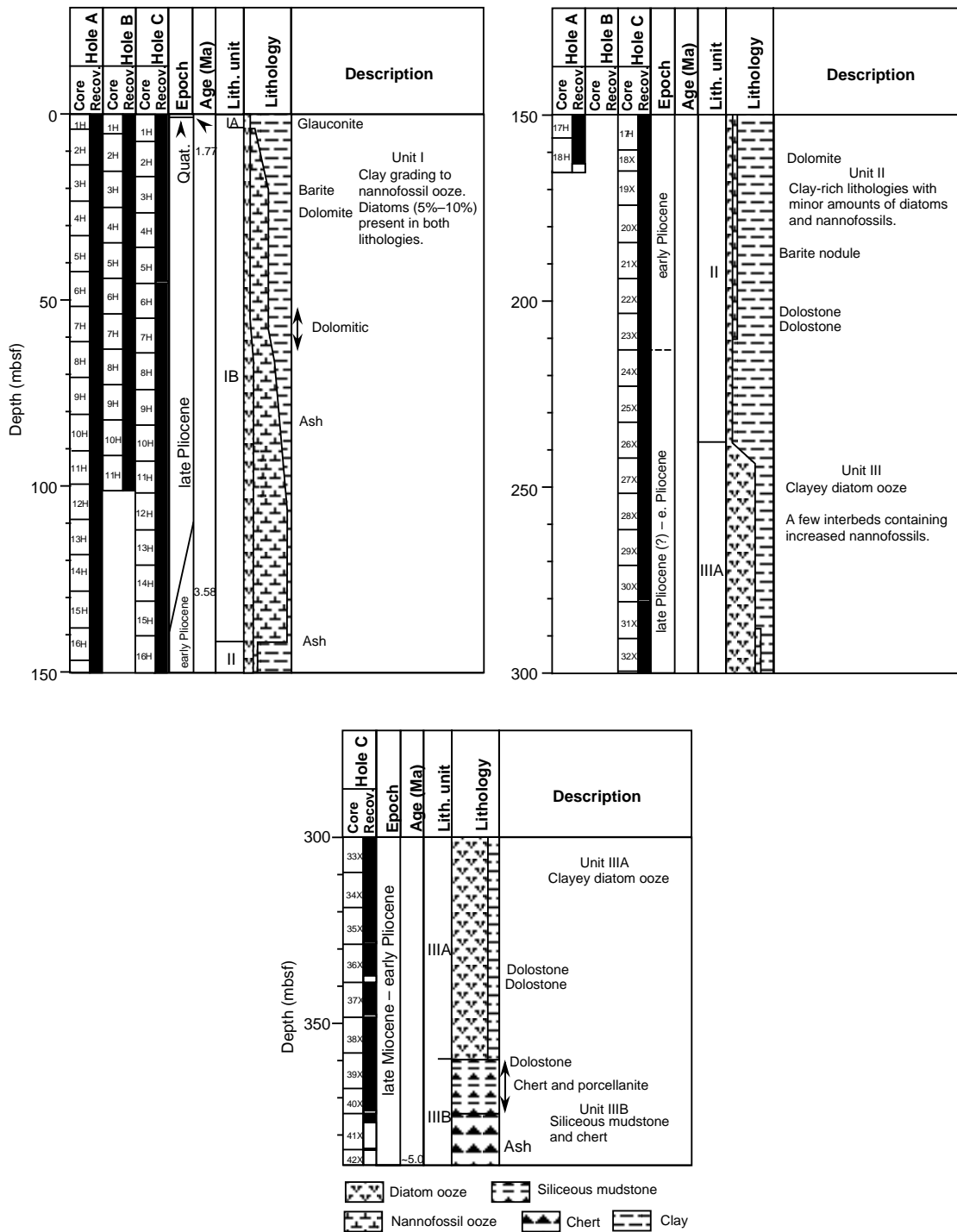


Figure 4. Site 1022 lithostratigraphic summary (0–387.7 mbsf).

atoms, and diatom clay. The uppermost part of the sequence is marked by a 1- to 3-m-thick bed of glauconitic clay that represents the entire Quaternary. The amount of nannofossils increases downward until nannofossil ooze and nannofossil clay mixed sediment are the dominant lithologies in the lower part of this unit. Dolomite, barite, and volcanic ash layers are each present at few horizons in this unit. Wood fragments are distributed throughout. Two subunits are recognized on the basis of nannofossil content and presence of glauconite sand pockets in the upper subunit.

Subunit IA

Hole 1022A, interval 167-1022A-1H-1 through 1H-C; 0–4.5 mbsf;
 Hole 1022B, interval 167-1022B-1H-1 through 1H-CC; 0–6.2 mbsf;
 Hole 1022C, interval 167-1022C-1H-1 through 1H-4; 0–6.0 mbsf.
 Age: Quaternary to late Pliocene, 0.0(?) to ~1.7 Ma.

Subunit IA consists of dark gray to olive gray (5Y 4/1 to 5Y 5/1) glauconitic clay with silt, pyrite, and diatoms overlying olive gray (5Y 4/2) clay with diatoms and silt. Fine to medium-grained glauco-

nite sand pockets occur frequently throughout this subunit. This coarser, glauconitic sediment is bioturbated down into the underlying clayey sediment, filling burrows therein. A few millimeter- to centimeter-sized fragments of wood are present. Only the uppermost few meters of sediment are Quaternary deposits. The base of this short unit is late Pliocene in age. The top of the underlying Subunit IB is marked by the continuous presence of >10% calcareous sediment.

Subunit IB

- Hole 1022A, interval 167-1022A-2H-1 through 15H-CC; 4.5–137.5 mbsf;
 Hole 1022B, interval 167-1022B-2H-1 through 11H-CC; 6.2–101.2 mbsf (bottom of hole);
 Hole 1022C, interval 167-1022C-1H-5 through 15H-CC; 6.0–140.5 mbsf.
 Age: late Pliocene, >2.3 to ~3.58 Ma.

Subunit IB is characterized by its significant calcareous nannofossil component. The upper boundary of Subunit IB is identified by the disappearance of glauconite sand pockets and the appearance of nannofossils. The upper part of this subunit is primarily composed of dark gray to olive gray (5Y 4/1 to 5Y 5/2) clay with nannofossils and diatoms, greenish gray to gray (5GY 4/2 to 5Y 5/1) diatom clay with silt, and gray (5Y 5/1) nannofossil diatom clay mixed sediment. Frequent occurrence of decimeter-thick disseminated glauconite intervals is observed down to approximately 35 mbsf. With increasing depth, the abundance of calcareous nannofossils increases until, by 80–90 mbsf, olive to light olive gray (5Y 5/3 to 5Y 6/2) nannofossil ooze with minor amounts of clay and diatoms is the predominant lithology. Smear-slide analyses indicate that the sediment is composed of 10%–70% nannofossils, 5%–50% diatoms, and 10%–70% clay. Important minor components include 2%–5% organic debris, 1%–3% pyrite, 2%–20% quartz, and 1%–10% foraminifers. Small, millimeter- to centimeter-scale fragments of wood are distributed throughout, but are most abundant above 58 mbsf. A few, thin vitric ash layers or pods are scattered through this subunit. Two pale yellow (5Y 7/3) barite-cemented horizons are present at 20 mbsf. Dolomite and dolomitic beds occur between 24–26 and 52–60 mbsf. Overall, the sediments grade from being slightly bioturbated and homogeneous in the upper part to being moderately bioturbated in the lower part of this subunit. *Chondrites* is the only identifiable trace fossil in evidence. The contact with the underlying Unit II is marked by an abrupt decrease in nannofossil content and corresponding increase in clay at approximately 140 mbsf.

Unit II

- Hole 1022A, interval 167-1022A-16H-1 through 18H-CC; 137.5–166.0 mbsf (base of hole);
 Hole 1022C, interval 167-1022C-16H-1 through 26X-2, 70 cm; 140.5–234.7 mbsf.
 Age: early Pliocene.

Unit II differs from the overlying unit by the predominance of clay with only minor amounts of silt, diatoms, and nannofossils (generally 5%–15% each). The major lithologies are dark gray to olive gray (5Y 4/1 to 5Y 4/2) clay with diatoms, silt, and nannofossils, diatom clay, and diatom clay mixed sediment with infrequent interbeds of gray to light olive gray (5Y 5/1 to 5Y 6/2) clayey nannofossil ooze. The silt-sized siliclastic component forms 3%–17% of the sediment and is made up almost entirely of quartz and feldspar. Together, diatoms and nannofossils generally compose less than 30% of the sediment, ranging from 2% to 40% and 1% to 47%, respectively. Foraminifers (1%–10%), pyrite (1%–6%), and organic matter (2%–4%) are the most important minor constituents. Well-indurated, olive gray to light olive gray (5Y 5/2 to 5Y 6/2) dolostone beds occur at 164, 202, and 206 mbsf. A 3-cm-diameter barite nodule at 185 mbsf was found near the top of a core and may be slough from uphole. Evi-

dence for bioturbation was limited because of the extreme fracturing and pulverization of sedimentary material by XCB coring. The contact with the underlying Unit III is marked by a gradual increase in diatom content beginning at approximately 235 mbsf.

Unit III

- Hole 1022C, interval 167-1022C-26X-2, 70 cm, through 42X-CC; 234.7–387.7 mbsf (bottom of hole).
 Age: Late Miocene to early Pliocene.

Unit III is predominantly biosiliceous in composition. The upper boundary of this unit is marked by a gradual change from diatom clay to clayey diatomite from ~235 to 245 mbsf. This unit is divided into two subunits based on the degree of diagenetic lithification. A diagenetic boundary was encountered at ~360 mbsf where diatomite is underlain by siliceous mudstone interbedded with decimeter-thick chert layers.

Subunit IIIA

- Hole 1022C, interval 167-1022C-26X-2 through 38X-CC; 234.7–357.8 mbsf.
 Age: late Miocene to early Pliocene.

This subunit is dominantly composed of dark gray to olive (5Y 4/1 to 5Y 4/3) diatomite and clayey diatomite. An approximately 10-m-thick interval of olive to pale olive (5Y 5/3 to 5Y 6/3) nannofossil diatomite with clay occurs in the middle part, and two thin dolostone beds occur in the lower part of this subunit. The diatomite is homogeneous to slightly bioturbated in general and moderately bioturbated in several intervals. Color changes are subtle and gradational. A sequence of thin laminations is present between ~293 and 295 mbsf.

Subunit IIIB

- Hole 1022C, interval 167-1022C-39X-1 through 42X-CC; 357.8–387.7 mbsf (bottom of hole).
 Age: late Miocene to early Pliocene.

The upper boundary of this subunit is marked by a 14-cm-thick layer of dolostone at the top of Core 167-1022C-39X, below which diatoms disappear and sediments are more lithified. This subunit is composed of olive gray (5Y 4/3 to 5Y 5/2) siliceous mudstone and porcellanite interbedded with decimeter-thick dark olive gray (5Y 3/2) chert layers. The shallowest chert occurs approximately at 368 mbsf. Siliceous mudstone is slightly bioturbated with centimeter-sized horizontal, flattened burrows.

BIOSTRATIGRAPHY

This report focuses on a description of the biostratigraphy of foraminifers, calcareous nannofossils, diatoms, and radiolarians of Holes 1022A and 1022B, representing the upper part (0(?)–166 mbsf) of the sequence at Site 1022. In addition, calcareous nannofossil biostratigraphy is described for Hole 1022C providing the only available age data for this hole.

Hole 1022A consists of 166 m of upper Pliocene through possible uppermost lower Pliocene sediments. Calcareous nannofossils and radiolarians suggest that the entire sequence is of late Pliocene age. On the other hand, the middle/late Pliocene boundary is recognized at 109 mbsf using planktonic foraminifers and at 138 mbsf using diatoms. The Quaternary is represented only by a very thin (<1 m) veneer of sediments overlying the late Pliocene. Hole 1022B consists of 101 m of late Pliocene sediments. The total age range of the sedimentary sequence recovered from Holes 1022A and 1022B is not well constrained. Planktonic foraminifers indicate that the top of the sequence is >2.25 Ma and that the base of Hole 1022A is older than 3.3 Ma. Calcareous nannofossils indicate that the age of the base of Hole

1022A is <3.8 Ma. Because the sequence is relatively thick, each of the four groups examined is represented by only one or two biozones, and few datums are recognized.

Calcareous nannofossils throughout Holes 1022A and 1022B are generally abundant and well preserved. Planktonic foraminifers are generally common to abundant throughout and moderately well preserved. Benthic foraminifers are continuously present in variable abundances. Radiolarians are rare to few but are well preserved. Diatoms are common to abundant and their preservation is poor to moderate, with most specimens exhibiting the effects of dissolution.

All of the microfossil groups in Holes 1022A and 1022B are represented by cool, relatively high-latitude assemblages. Radiolarians are entirely represented by subarctic forms. Diatoms are dominated by north Pacific subarctic assemblages. Discoasters are absent above the middle upper Pliocene (younger than 2.7 Ma). Below this they are rare. Planktonic foraminifer assemblages are dominated by subarctic to cool temperate forms, with subtropical elements absent.

Both diatoms and radiolarians show evidence of strong upwelling throughout the Pliocene. The sequence at Site 1022 is the most diatomaceous of late Pliocene age of all Leg 167 sites. Radiolarians indicate a prevalence of strong coastal upwelling, while the diatoms reflect oscillations between strong coastal upwelling (as marked by abundant, large *Coscinodiscus*) and oceanic upwelling (as marked by abundant *Thalassiothrix*). Benthic foraminifers found throughout are typical, middle bathyal deep-sea assemblages indicative of well-oxygenated bottom waters.

Hole 1022C consists of 384 m of upper Pliocene through undifferentiated early Miocene/late Miocene sediments. As in Hole 1022A, the Quaternary is represented by the uppermost ~1 m of the sequence. The middle/late Miocene boundary in Hole 1022C is recognized at 165.20 mbsf based on calcareous nannofossils.

Planktonic Foraminifers

Holes 1022A and 1022B contain a moderately good and apparently continuous record of upper to uppermost middle Pliocene plank-

tonic and benthic foraminifers (Table 3). The Quaternary and uppermost Pliocene are missing at Site 1022 because of the presence of an unconformity at or close to the ocean floor. Planktonic foraminifers indicate that the base of Hole 1022A is of latest early Pliocene age (>3.3 Ma) and that the top of the sequence is of late Pliocene (>2.25 Ma) age. Planktonic foraminifers are generally common to abundant throughout and are moderately well preserved. Benthic foraminifers are continuously present in variable abundances. Planktonic foraminifer assemblages are similar to those of the same age in other sites off the northern California margin. The only planktonic foraminifer datum recorded in Hole 1022A is the FO of *Globorotalia inflata* (109 mbsf; Sample 167-1022A-12H-CC) with an assigned age of 3.3 Ma. This datum is taken as the boundary between the early and late Pliocene. The early Pliocene at Hole 1022A is bracketed by the occurrence of *Globigerina decoraperta*. Benthic foraminifer assemblages, however, are represented by typical middle bathyal oceanic forms that lived in well-oxygenated environments.

Calcareous Nannofossils

In Holes 1022A and 1022B, calcareous nannofossils are generally abundant and well-preserved. Below 138 mbsf in Hole 1022A, they exhibit traces of etching (Table 4). Discoasters in the upper upper Pliocene are rare or absent because of the relatively cool conditions. Below this interval (~2.6–2.7 Ma), they are rare to few. Hole 1022A spans late Pliocene Zone CN12a to Pleistocene Zone CN14a. Hole 1022B ranges from late Pliocene Zone CN 12a to late Pleistocene Zone CN15. Quaternary sediments in both holes are represented by approximately the uppermost meter. Quaternary calcareous nannofossil assemblages are marked by the presence of *Emiliania huxleyi*, *Pseudoemiliania lacunosa*, *Calcidiscus leptoporus*, and several morphotypes of *Gephyrocapsa* spp. Quaternary sediments are separated from those of Pliocene age in the interval between Samples 167-1022A-1H, 100 cm, and 1H-2, 125 cm, in Hole 1022A, and between Samples 167-1022B-1H, 91 cm, and 1H-CC in Hole 1022B. Pliocene nannofossil assemblages are marked by an association of *Heli-*

Table 3. Distribution and relative abundances of planktonic foraminifers in Hole 1022A.

Zone	Core, section, interval	Depth (mbsf)	Abundance	Preservation	<i>Globorotalia inflata</i>	<i>Globorotalia scitula</i>	<i>Globorotalia</i> cf. <i>conomiotoza</i>	<i>Globigerina decoraperta</i>	<i>Neogloboquadrina</i> cf. <i>continuuosa</i>	<i>Neogloboquadrina asanoi</i>	<i>Neogloboquadrina humerosa</i>	<i>Neogloboquadrina</i> sp. "rounded"	<i>Neogloboquadrina pachyderma</i> dex.	<i>Globigerina bulloides</i>	<i>Globigerina woodi</i>	<i>Globigerina apertura</i>	<i>Orbulina universa</i>	<i>Globigerinoides ruber</i>
N21	167-1022A-1H-CC	5	A	M						A	C	C	C	A				
	2H-CC	16	A	M	C					A	F			A				
	3H-CC	24	C	M	A									A				
	4H-CC	33	F	P										A			F	
	5H-CC	43	C	M	C									A				
	6H-CC	52	A	M	R					A	F	A	A	A				
	7H-CC	62	C	M	R						F	A	C	A				F
	8H-CC	71	A	G	F						A	A	A	A				F
	9H-CC	81	C	M	A									F				R
	10H-CC	90	C	M	R							C	F	A				R
	11H-CC	100	A	G									A	F				C
	12H-CC	109	A	G	A									A				A
N20	13H-CC	119	A	M				C						A				F
	14H-CC	128	R	P										F				R
	15H-CC	138	C	M			R				F	R	F	A				R
	16H-CC	147	R	P					R		R		R	C				R
	17H-CC	157	R	P									R	F				R
	18H-CC	166	F	M				C					F	C	F	F		C

Note: See "Explanatory Notes" chapter for abbreviations.

Table 4. Distribution and relative abundances of calcareous nannofossils in Holes 1022A and 1022B.

Zone	Core, section, interval (cm)	Depth (mbsf)	Preservation	Abundance	<i>Emiliana huxleyi</i>	<i>Pseudoemiliana lacunosa</i>	<i>Helicosphaera carteri</i>	<i>Helicosphaera sellii</i>	<i>Gephyrocapsa oceanica</i> s.l.	<i>Gephyrocapsa</i> sp. 3	<i>Gephyrocapsa</i> small	<i>Gephyrocapsa</i> large	<i>Discoaster brouweri</i>	<i>Discoaster pentaradiatus</i>	<i>Discoaster surculus</i>	<i>Discoaster tamalis</i>	<i>Discoaster asymmetricus</i>	<i>Ceratholithus</i> spp.	<i>Coccolithus pelagicus</i>	<i>Calcidiscus macintyreii</i> >11 µm	<i>Calcidiscus leptoporus</i>
CN14a	167-1022A-1H-1, 50	0.50		B																	
	1H-1, 100	1.00	G	A	C				R/F	A											C
	1H-2, 50	2.00	P	RR						R											
	CN13a–CN12 1H-2, 125	2.75	M/G	A	P														R	P	C
	CN13a–CN12 1H-3, 50	3.50	M/G	A	C	F/C	C													P	C
	CN13a–CN12 1H-3, 120	4.20	G	A	C	C	C												F	R	C
	CN13a–CN12 1H-CC	4.50	M	C/A	F		C	R												R	C
	CN13a–CN12 2H-CC	14.00	P	F	P														F	R	R
	CN12 3H-CC	23.50	P/M	C	P										R					R	R
	CN12 4H-CC	33.00	P	R	P										R	R					
	CN12 5H-CC	42.50	G	A	P									R	R						
	CN12 6H-CC	52.00	G	A										R	R						
	CN12 7H-CC	61.50	G	A										R	R				F	P	C
	CN12a 8H-CC	71.00	G	A										R	R						C
	CN12a 9H-CC	80.50	G	A		R/F								R	R				F	C	C
	CN12a 10H-CC	90.00	G	A		F								R	R					C	C
	CN12a 11H-CC	99.50	G	A		C								R	R					F/R	C
	CN12a 12H-CC	109.00	G	A		P								R	R	R				F	P
CN12a 13H-CC	118.50	G	A		R		R							R	R		R		F	C	
CN12a 14H-CC	128.00	G	A		P		P							R	F/R	F/R		R	R	F	
CN12a 15H-CC	137.50	M/G	A		P							R	R		R				C/F	C	
CN12a 16H-CC	147.00	P/M	C/A		R									R					R	P	
CN12a 17H-CC	156.50	P/M	F/C												P			R	F	R	
CN12a 18H-CC	166.00	G	C		P		R								F				R	R	
CN15	167-1022B-1H-1, 22	0.50	P	F	R			P		P										C	
	CN14a 1H-1, 91	0.91	G	A		R/F		C		A											P
	CN13a–CN12 1H-CC	6.20	P/M	C		R		R												F	F
	CN13a–CN12 2H-CC	15.70	M/G	A		F	R													F	F
	3H-CC	25.20		B																	
	CN13a–CN12 4H-CC	34.70	M	C		P		R													F
	CN12 5H-CC	44.20	P	RR											R						
	CN12 6H-CC	53.70	M/G	A		C									R				F	R	
	CN12 7H-CC	63.20	G	A											R				F	R	C
	CN12 8H-CC	72.70	M/G	A										F	R				C	R	C
	CN12 9H-CC	82.20	G	A		C								R	P				C	R	C
CN12 10H-CC	91.70	G	A		C	P	R						R	R					R	C	
CN12a 11H-CC	101.20	G	A		C									R				P	R	C	

Note: See "Explanatory Notes" chapter for abbreviations.

cosphaera carteri, *H. sellii*, *Discoaster brouweri*, *D. tamalis*, *D. pentaradiatus*, *D. surculus*, and several morphotypes of *Reticulofenestra*.

In Hole 1022C, calcareous nannofossils are generally abundant and well preserved until 203.6 mbsf, below which they are rare and poorly preserved (Table 5). Discoasters in the uppermost Pliocene are rare to few. Hole 1022C spans early Pliocene/late Miocene Zone CN9–CN11 to late Pleistocene Zone CN15–CN14b. Quaternary sediments are represented by the upper ~1 m. Quaternary calcareous nannofossil assemblages are marked by the presence of *Emiliana huxleyi*, *Pseudoemiliana lacunosa*, *Calcidiscus leptoporus*, and several morphotypes of *Gephyrocapsa* spp. The boundary between the Pliocene and the Quaternary occurs between Samples 167-1022C-1H, 90 cm, and 167-1022C-1H-CC. Pliocene nannofossil assemblages are marked by an association of *Helicosphaera carteri*, *H. sellii*, *Discoaster brouweri*, *D. tamalis*, *D. pentaradiatus*, *D. surculus*, *Amaurolithus* spp., and several morphotypes of *Reticulofenestra*. The lower/upper Pliocene boundary, which is close to the LO of *Reticulofenestra pseudoumbilicus* (base of CN12a), occurs between Samples 167-1022C-18X-CC and 167-1022C-19X-CC.

Because many marker species are absent or rare in the lower Pliocene through upper Miocene sediments, it is difficult to develop a precise biostratigraphic assignment of this part of the sequence. The presence of *Amaurolithus* spp. from Samples 167-1022C-19X-CC to

38X-CC, however, allows assignment of this interval to Zones CN11–CN9 (undifferentiated upper Miocene/lower Pliocene).

Diatoms

Diatoms are generally common to abundant and poorly to moderately well preserved all through the sequence. Pliocene diatom assemblages recovered from Hole 1022A are made up of cool temperate to subarctic taxa, and most specimens are etched as a result of strong dissolution. The standard North Pacific diatom zonation has been used at Hole 1022A (Table 6). Littoral forms and reworked assemblages are not significant at this site.

In the Pliocene, diatom assemblages are marked by the presence of *Neodenticula seminae*, *Neodenticula koizumii*, and *Neodenticula kamschatica*. The late Pliocene zonal boundary between the NPD 9 and the NPD 8 Zones is difficult to place because of very rare occurrences of *N. kamschatica*. The boundary is tentatively placed at the LCO of *N. kamschatica* between Samples 167-1022A-9H-CC and 10H-CC. The lower/upper Pliocene boundary, which is close to the FO of *N. koizumii* (top of the NPD 7c), occurs between Samples 167-1022A-15H-CC and 16H-CC. Diatom species characteristic of upwelling conditions are sometimes dominant throughout the sequence, exhibiting clear oscillations associated with oceanic/coastal environmental changes as reflected by the diatom assemblages.

Table 5. Distribution and relative abundances of calcareous nannofossils in Hole 1022C.

Zone	Core, section, interval (cm)	Depth (mbsf)	Preservation	Abundance	<i>Emiliania huxleyi</i>	<i>Pseudoemiliania lacunosa</i>	<i>Helicosphaera carteri</i>	<i>Helicosphaera sellii</i>	<i>Gephyrocapsa oceanica</i> s.l.	<i>Gephyrocapsa</i> small	<i>Discosaster braueri</i>	<i>Discosaster pentaradiatus</i>	<i>Discosaster surculus</i>	<i>Discosaster tamalis</i>	<i>Discosaster asymmetricus</i>	<i>Sphenolithus</i> spp.	<i>Reticulofenestra pseudoumbilicus</i>	<i>Amaurolithus</i> spp.	<i>Coccolithus pelagicus</i>	<i>Calcidiscus macintyrei</i> > 11 µm	<i>Calcidiscus leptoporus</i>
CN15–CN14b	1022C-1H-1, 21	0.21	P	R	R																
CN14a	1H-1, 90	0.90	M/C	C		R/F				P											P
CN13a–CN12	1H-CC	7.50	M/C	C		C				A											R
	2H-CC	17.00		B																	
CN12	3H-CC	26.50	M	C						RR									F		R
CN12	4H-CC	36.00	P	R		P															F
CN12	5H-CC	45.50	M/G	C/A		P															R
CN12	6H-CC	55.00	G	A		P															R
CN12	7H-CC	64.50	G	A		F															R
CN12a	8H-CC	74.00	G	A		C				R											R
CN12a	9H-CC	83.50	G	A		C		R			R/F										R
CN12a	10H-CC	93.00	G	A		R				R											R
CN12a	11H-CC	102.50	G	A		P		R													R
CN12a	12H-CC	112.50	G	A		P	R	R													R
CN12a	13H-CC	121.50	G	A		C															R
CN12a	14H-CC	131.00	G	A		P					R										R
CN12a	15H-CC	140.50	G	C		C					R										R
CN12a	16H-CC	150.00	G	A		P					R										R
CN12a	17H-CC	159.50	M	C		R	R	R													R
CN12a	18X-CC	165.20	G	A		R									R						R
CN11–CN9	19X-CC	174.80	P/M	C				RR			RR							cf	C		R
CN11–CN9	20X-CC	184.00	P	R			R	R			P							R	R		R
CN11–CN9	21X-CC	194.00	P	A							R							R	R		R
CN11–CN9	22X-CC	203.60	G	A			R				R							R	R		R
CN11–CN9	23X-CC	213.20	P	R			RR				R							R	R		R
	24X-CC	222.90		B																	
	25X-CC	232.50	P	RR													RR	RR	R	P	
	26X-CC	242.10		B																	
	27X-CC	251.80		B																	
	28X-CC	261.40		B																	
	29X-CC	271.00	P	RR																	
CN11–CN9	30X-CC	280.60	P	R																	R
CN11–CN9	31X-CC	290.30	P	R/F							R										R
CN11–CN9	32X-CC	299.90	P/M	C/A																	R
CN11–CN9	33X-CC	309.60	P	F/C																	R
	34X-CC	319.30		B																	
	35X-CC	328.90		B																	
	36X-CC	338.60		B																	
CN11–CN9	37X-CC	348.20	P	F/R																	R
CN11–CN9	38X-CC	357.99	P	RR																	R
	39X-CC	367.70		B																	
	40X-CC	373.53		B																	
	41X-CC	375.89		B																	
	42X-CC	383.80	P	R																	R

Note: See “Explanatory Notes” chapter for abbreviations.

Radiolarians

Radiolarians are rare to few and well preserved in all core catchers from Hole 1022A (Table 7). The occurrence of *Lamprocyrtis neoheteroporos* and *L. heteroporos*, and the absence of *Eucyrtidium matuyamai* gives an upper Pliocene age (>2 Ma.) to Sample 167-1022A-2H-CC (14 mbsf). The evolutionary transition between *L. neoheteroporos* and *L. heteroporos* between 2.6–2.8 Ma cannot be placed because the assemblages have such low diversity. The LO of *Anthocyrtidium pliocenica* (3.3 Ma) was recognized between Samples 167-1022A-11H-CC (99.5 mbsf) and 12H-CC (109 mbsf). The base of the hole cannot be dated.

Radiolarian assemblages are characterized by very low diversity. Subarctic species are predominant. Occurrences of many species characteristic of upwelling conditions are common throughout the sequence suggesting constant vertical advection of deep waters.

PALEOMAGNETISM

We made magnetic measurements with the pass-through cryogenic magnetometer on the archive halves of APC cores from Hole 1022A. The natural remanent magnetization (NRM) was measured on the top 3 cores (0 to 23.5 mbsf). Time constraints dictated that the remaining cores be measured only after alternating field (AF) demagnetization. An AF demagnetization of 20 mT was used in the top 12 mbsf of Hole 1022A, but proved too high, removing too much of the weak NRM. The 15 mT AF field applied below 12 mbsf represented a compromise between removing the drilling overprint and leaving a detectable magnetization. In the investigated 16 APC cores, the remanent magnetization after AF demagnetization mostly ranged between 0.03 and 5 mA/m (Fig. 5). In the interval between 1 and 24 mbsf the magnetization was very low. The sensitivity of the magnetometer seems to vary on a daily basis and, at this site, seemed to be at about 0.2 mA/m, based on measurements of sections of the core that had been turned by 180°.

According to biostratigraphic data, Hole 1022A consists mostly of late Pliocene sediments, and the Quaternary is represented only by a thin veneer of surface sediments (see “Biostratigraphy” section, this chapter). The negative or shallow inclinations in Cores 167-1022A-2H and 3H may correspond to the reversed polarity Chron C2r, but the very low magnetic intensity of this interval does not allow a reliable correlation. The inclinations after demagnetization were mainly positive between 24 and 142 mbsf. The normal polarity throughout most of this hole is most likely caused by a secondary overprint and does not represent the primary magnetization. As shown in Figure 5, stepwise changes of inclination and intensity were often observed at core boundaries, and declination values are mostly confined around 0°. These discontinuities at core boundaries suggest that a drilling-induced overprint is prevailing in most intervals.

COMPOSITE DEPTHS AND SEDIMENTATION RATES

Multisensor track (MST) data collected at 4- to 10-cm intervals from Holes 1022A through 1022C, and color reflectance data collected at 6-cm intervals from Holes 1022A and 1022B were used to determine depth offsets in the composite section. On the composite depth scale (expressed as mcd, meters composite depth), features of the plotted MST and color reflectance data present in adjacent holes are aligned so that they occur at approximately the same depth. Working from the top of the sedimentary sequence, a constant was added to the mbsf (meters below sea floor) depth for each core in

each hole to arrive at a mcd depth for that core. The depths offsets that comprise the composite depth section are given in Table 8. The continuity of the sedimentary sequence was documented for the upper 170 mcd, equivalent to the interval that was multiple cored.

Magnetic susceptibility, GRAPE density, and color reflectance measurements were the primary parameters used for interhole correlation purposes. Natural gamma-ray activity measurements were made throughout the entire section in Hole 1022A and from Core 167-1022C-19X to the base of the section in Hole 1022C, but the sampling interval of 12 cm was insufficient for interhole correlation.

The magnetic susceptibility, color reflectance, and GRAPE density records used to verify core overlap for Site 1022 are shown on a composite depth scale in Figures 6, 7, and 8, respectively. The GRAPE data were used to identify intervals of voids and highly disturbed sediments (values less than 1.50 g/cm³) and all MST and color reflectance data were culled from these intervals. The cores from Holes 1022A through 1022C provide continuous overlap to about 170 mcd. The composite records suggest that up to 2.5 m of material may be missing between cores down to about 170 mcd, although the average gap is about 1 m. As there are no data to fill possible core gaps below 170 mcd, an assessment of core gap length below this depth is not possible.

Following construction of the composite depth section for Site 1022, a single spliced record was assembled from the aligned cores mainly using magnetic susceptibility and GRAPE data and, in some cases, color reflectance data. Cores from Hole 1022A were used as the backbone of the sampling splice. Cores from Holes 1022B and 1022C were used to splice across core gaps in Hole 1022A. The composite depths were aligned so that tie points between adjacent holes occurred at exactly the same depths in meters composite depth. The Site 1022 splice (Table 9) can be used as a sampling guide to recover a single sedimentary sequence that is continuous down to 170 mcd. Intervals having significant disturbance or distortion were avoided if possible. Core 167-1022C-13H had flow-in structures in Sections 3 through 5. Unfortunately, a 1.12 m interval of Section 167-1022C-13H-5 had to be used in the splice as no other core material from Holes 1022B and 1022C was available to cover the core gap in Hole 1022A. In general, many of the splice ties at this site should be considered tentative until further postcruise processing of the data is conducted.

INORGANIC GEOCHEMISTRY

We collected 10 interstitial water samples from Hole 1022A at depths ranging from 2.95 to 160.95 mbsf. We also collected seven interstitial water samples from Hole 1022C at depths ranging from 188.85 to 326.25 mbsf. Because of limited time near the end of the leg, the Hole 1022C samples were only analyzed on board ship for alkalinity, pH, and salinity. The results from Hole 1022A are described in the following. Chemical gradients in the interstitial waters at this site (Tables 10, 11) reflect organic matter diagenesis, the dissolution of biogenic opal and calcium carbonate, authigenic mineral precipitation, and the diffusive influence of reactions in the underlying basalt.

Chlorinity increases by 1.8% from 550 mM at 2.95 mbsf to approximately 560 mM from 18.45 to 37.45 mbsf, then decreases with increasing depth to values around 550 mM from 103.99 to 160.95 mbsf (Fig. 9). Salinity, measured refractively as total dissolved solids, ranges from 32.0–34.5. Sodium concentrations measured by flame emission spectrophotometry were on average <3% lower than those estimated by charge balance (Table 10).

Alkalinity increases to >15 mM from 37.45 to 160.95 mbsf (Fig. 9). Sulfate concentrations decrease to values below the detection lim-

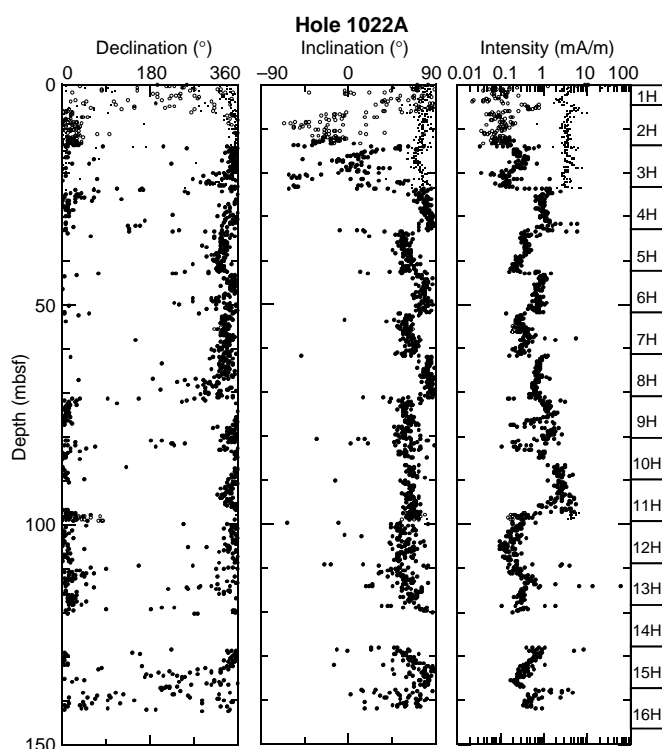


Figure 5. Plots of magnetic declination, inclination, and intensity of APC cores from Hole 1022A. Small and large dots represent data before and after AF demagnetization, respectively. Solid and open symbols show the results after AF demagnetization at 15 and 20 mT, respectively.

it (<0.4 mM) by 37.45 mbsf, with the sulfate decrease coincident with the alkalinity increase. Phosphate concentrations are >65 μM from 27.95 to 46.95 mbsf, then decrease with increasing depth at first steeply, then more gradually, to 8 μM at 160.95 mbsf. Ammonium concentrations increase steadily with increasing depth to 5.7 mM at 160.95 mbsf.

Dissolved silicate concentrations are 700–910 μM from 2.95 to 18.45 mbsf and then increase with depth to values >1000 μM from 27.95 to 75.45 mbsf, indicative of the dissolution of biogenic opal; they decrease to slightly lower values at greater depths (Fig. 9). Strontium concentrations increase to 182 μM at 160.95 mbsf.

Calcium concentrations decrease to a minimum of 4.1 mM at 37.45 mbsf, then increase with increasing depth to 6.4 mM at 160.95 mbsf (Fig. 9). The average calcium gradient from the depth of the calcium minimum is +1.9 mM/100 m. Magnesium concentrations decrease throughout to 23.4 mM at 160.95 mbsf, with an average gradient from the depth of the calcium minimum of -8.8 mM/100 m. The decrease in dissolved calcium in the upper sediment indicates that authigenic mineral precipitation may be significant in influencing this profile in this depth range, while both profiles apparently reflect the diffusive influence of reactions in underlying basalt at deeper depths. At depths ≥ 37.45 mbsf, the calcium increase is linearly correlated to the magnesium decrease, with $\Delta\text{Ca}/\Delta\text{Mg}$ of -0.21 ($R^2 = 0.88$). Potassium concentrations decrease with increasing depth to 8.7 mM at 160.95 mbsf (Table 10). Lithium concentrations increase with increasing depth to 167 μM at 160.95 mbsf (Fig. 9).

ORGANIC GEOCHEMISTRY

Organic geochemical analyses performed at Site 1022 include measurements of elemental composition and volatile hydrocarbons

Table 8. Site 1022 composite depth section.

Core, section	Depth (mbsf)	Offset (m)	Depth (mcd)
167-1022A-			
1H-1	0	0.12	0.12
2H-1	4.5	0.44	4.94
3H-1	14	1.16	15.16
4H-1	23.5	0.11	23.61
5H-1	33	0.09	33.09
6H-1	42.5	1.83	44.33
7H-1	52	2.55	54.55
8H-1	61.5	4.76	66.26
9H-1	71	4.97	75.97
10H-1	80.5	4.54	85.04
11H-1	90	5.46	95.46
12H-1	99.5	5.48	104.98
13H-1	109	5.85	114.85
14H-1	118.5	7.52	126.02
15H-1	128	9.42	137.42
16H-1	137.5	9.7	147.2
17H-1	147	12.94	159.94
18H-1	156.5	12.94	169.44
167-1022B-			
1H-1	0	0	0
2H-1	6.2	0.04	6.24
3H-1	15.7	1.74	17.44
4H-1	25.2	0.35	25.55
5H-1	34.7	1.89	36.59
6H-1	44.2	1.59	45.79
7H-1	53.7	3.89	57.59
8H-1	63.2	4.3	67.5
9H-1	72.7	4.16	76.86
10H-1	82.2	3.68	85.88
11H-1	91.7	3.68	95.38
167-1022C-			
1H-1	0	0	0
2H-1	7.5	0	7.5
3H-1	17	0.56	17.56
4H-1	26.5	-0.01	26.49
5H-1	36	-0.06	35.94
6H-1	45.5	0.27	45.77
7H-1	55	3.33	58.33
8H-1	64.5	4.4	68.9
9H-1	74	4.46	78.46
10H-1	83.5	4.65	88.15
11H-1	93	5.1	98.1
12H-1	102.5	5.13	107.63
13H-1	112	5.63	117.63
14H-1	121.5	7.13	128.63
15H-1	131	7.51	138.51
16H-1	140.5	10.02	150.52
17H-1	150	10.98	160.98
18X-1	159.5	10.98	170.48
19X-1	165.2	10.98	176.18

Note: This table is also on CD-ROM, back pocket, this volume.

(for methods see “Organic Geochemistry” section, “Explanatory Notes” chapter, this volume).

Volatile Hydrocarbons

As part of the shipboard safety and pollution program, volatile hydrocarbons (methane, ethane, and propane) in the sediments at Site 1022 were routinely measured by gas chromatography. Results are presented in Table 12 and Figure 10. Headspace methane concentrations increased gradually from 0 and 38 mbsf and were almost constant (more than 10,000 ppm) below 38 mbsf. The methane/ethane (C_1/C_2) ratio increased from 0 to 66 mbsf and then decreased downhole to about 400. The high C_1/C_2 ratios indicate that the methane is of biogenic origin. Higher weight molecular hydrocarbon gases up to C_6 were observed. In contrast to previous sites, C_4 to C_6 were present at shallow depths (~100 mbsf). These hydrocarbons probably migrated from thermally matured sediments.

Elemental Analysis

At Site 1022, 59 sediment samples were analyzed for total carbon, inorganic carbon, total nitrogen, and total sulfur (Fig. 11; Table 13).

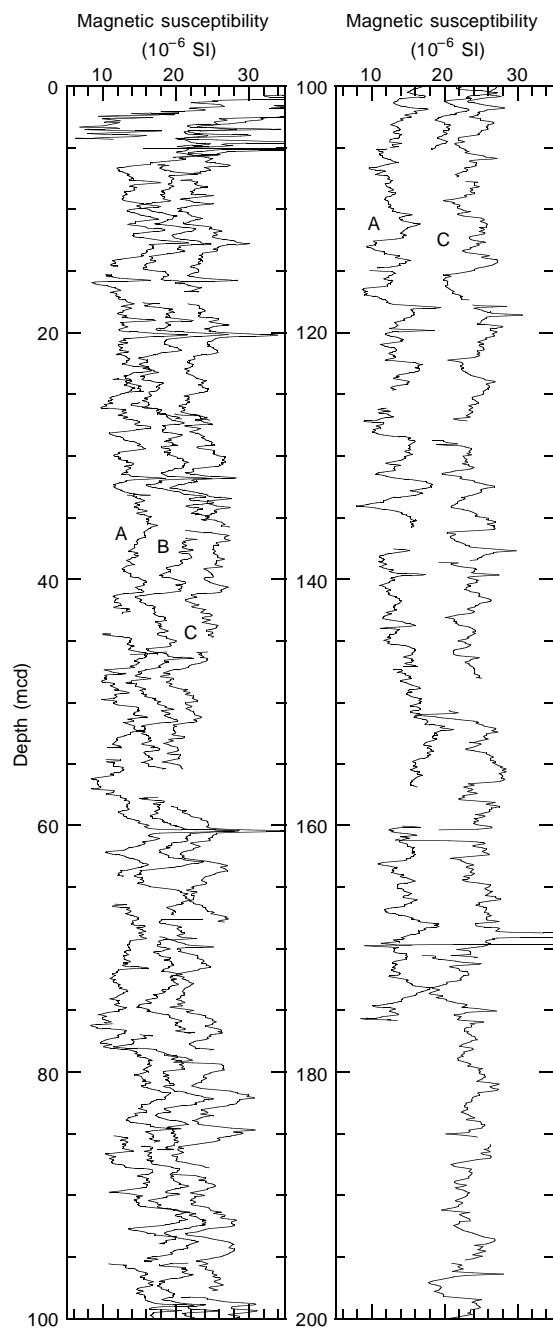


Figure 6. Smoothed (15-cm Gaussian) magnetic susceptibility data for the upper 200 m from Site 1022 on the mcd scale. Holes 1022A, 1022B, and 1022C are offset from each other by a constant (5×10^{-6} SI).

The percentage of calcium carbonate (CaCO_3) was calculated from inorganic carbon concentrations by assuming that all carbonate occurs in the form of calcite. The calcium carbonate contents vary between ~1 and 47 wt% (Table 13; Fig. 11). A single spike with high CaCO_3 content (47 wt%) is observed at 25.9 mbsf. Overall, the CaCO_3 content generally increases downwards in Unit I, which coincides with the lithology (see “Lithostratigraphy” section, this chapter). After a maximum at ~105 mbsf, the values decrease again to 5 wt% at the boundary of Unit I and Unit II.

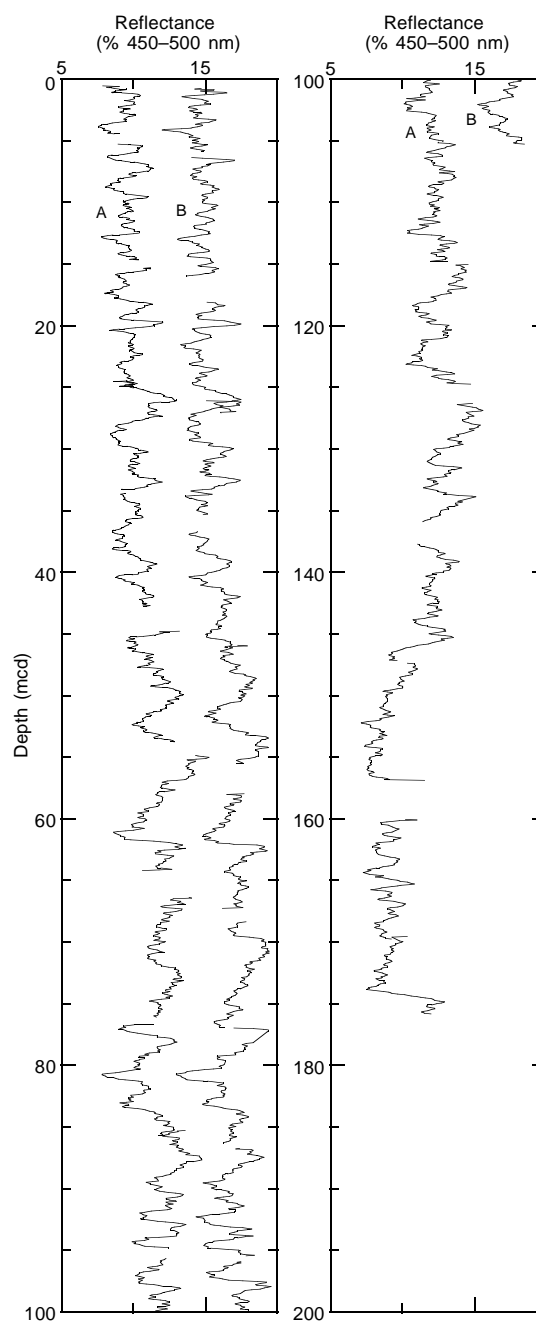


Figure 7. Smoothed (15-cm Gaussian) color reflectance (% 450–500 nm band) data for the upper 200 m from Site 1022 on the mcd scale. Holes 1022A and Hole 1022B are offset from each other by a constant (5%).

The total organic carbon (TOC) content at Site 1022 varies between 0 and 1.5 wt% (Table 13; Fig. 11) and shows very constant values in lithostratigraphic Unit I. In Unit II, the values slightly increase. One sample with 0 wt% organic carbon at 42 mbsf was taken in an ash layer.

Total nitrogen content varies between 0.09 and 0.40 wt%, and total sulfur content ranges from 0 to ~10.4 wt% (Table 13). The high sulfur content (10.4 wt%) of Sample 167-1022A-15H-1, 29–30 cm, reflects the accumulation of pyrite in the sediment. Most of the total

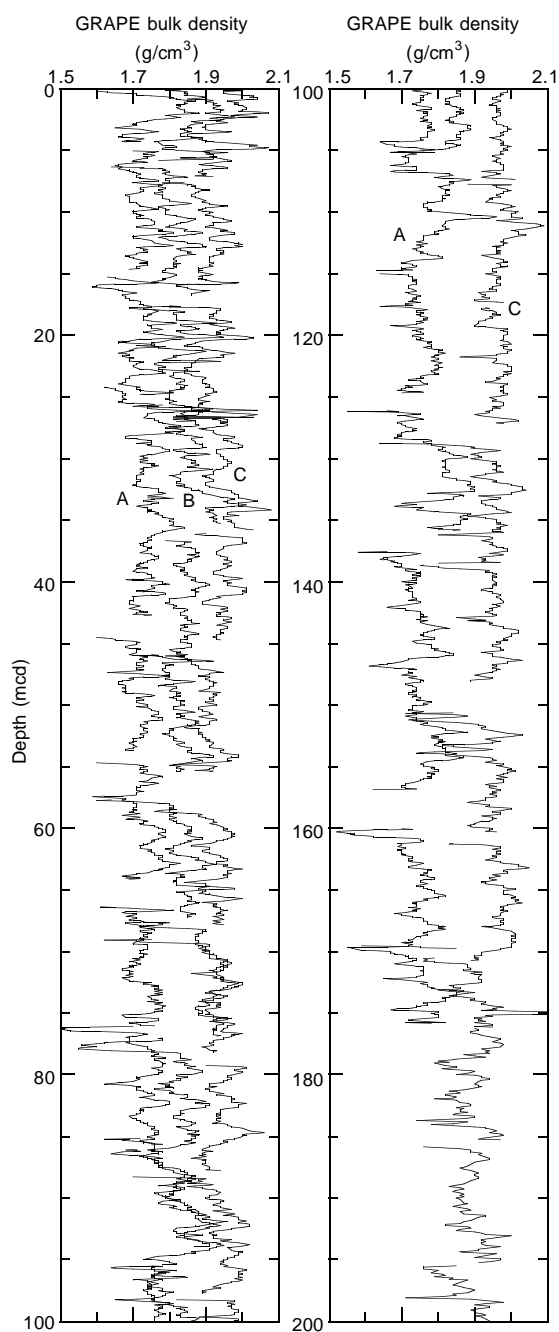


Figure 8. Smoothed (15-cm Gaussian) GRAPE bulk density data for the upper 200 m from Site 1022 on the mcd scale. Holes 1022A, 1022B, and 1022C are vertically offset from each other by a constant (0.1 g/cm^3).

organic carbon/total nitrogen (TOC/TN) ratios range between 5 and 9, indicating a predominantly marine origin of the organic material (Bordovskiy, 1965; Emerson and Hedges, 1988).

PHYSICAL PROPERTIES

Multisensor Track Measurements

The shipboard physical properties program at Site 1022 included nondestructive measurements of bulk density, magnetic susceptibili-

ty, *P*-wave velocity, and natural gamma-ray activity on whole sections of all cores using the MST (Fig. 12). Magnetic susceptibility was measured at 4-cm intervals at low sensitivity (1-s measuring time) on all Site 1022 cores. GRAPE bulk density measurements were made at 4-cm intervals on all cores from Site 1022. PWL velocity measurements were made at 4-cm intervals to about 60 mbsf in each Site 1022 hole. Natural gamma-ray activity was measured with a 15-s count every 12 cm on cores from Holes 1022A and 1022C.

Index Properties

Index properties measurements were made at three samples per working core on all cores from Hole 1022A. The index properties bulk density, void ratio, porosity, water content, dry-bulk density, and grain density (Fig. 13) were determined using gravimetric Method C (Table 14 on CD-ROM in the back pocket of this volume).

Compressional-Wave Velocity

Sonic velocity was measured with the Hamilton Frame of the digital sonic velocimeter (pair T3, in the x-direction) to a depth of 50.82 mbsf in Hole 1022A at an average of one per section (Table 15 on CD-ROM in the back pocket of this volume).

Heat Flow

Thermal conductivity was measured to 77.25 mbsf in Hole 1022A (Table 16 on CD-ROM in the back pocket of this volume). Three downhole temperature measurements were taken with the APC Adara temperature tool in Hole 1022A: 4.7°C at 33.0 mbsf, 6.8°C at 52.0 mbsf, and 8.0°C at 71.0 mbsf in Cores 167-1022A-4H, 6H, and 8H, respectively (Fig. 14). Bottom-water temperature was measured on all runs, indicating a bottom-water temperature of $1.9^\circ \pm 0.1^\circ\text{C}$. The four data points yield a thermal gradient of 88°C/km (Fig. 15). Using an average measured thermal conductivity of $0.950 \text{ W/(m}\cdot\text{K)}$ provides a heat-flow estimate of 84 mW/m^2 at Site 1022.

Color Reflectance

Reflectance measurements were taken at 4- to 6-cm intervals on cores from Holes 1022A and 1022B. Time constraints precluded shipboard measurement of color reflection below 162 mbsf in Hole 1022A. A summary of the 450–500-nm band average (blue) for Hole 1022A is given in Figure 16. From 0 to 120 mbsf in lithostratigraphic Unit I, color reflectance rises gradually from approximately 9% to 14%, a function of increasing nannofossil abundance with depth. Throughout this interval, reflectance displays cyclicity with wavelengths averaging 5–10 m. At approximately 140 mbsf, the boundary between lithostratigraphic Units I and II, color reflectance drops abruptly to 8%, consistent with the shift from clayey nannofossil ooze to clay with diatoms and nannofossils.

Digital Color Video

Cores from all holes at Site 1022 were imaged with the ODP color digital imaging system at 20-cm intervals downcore, providing a 0.25-mm pixel. Video images of color CIELAB L^* from Holes 1022A and 1022B are shown in Figure 17.

DOWNHOLE MEASUREMENTS

Logging Operations and Log Quality

Hole 1022C was logged with the density-porosity combination, sonic-FMS, and GHMT tool strings after the hole was flushed of debris and the drill pipe was set at 80 mbsf (Table 17). Two full passes

Table 9. Site 1022 splice tie points.

Hole, core, section, interval (cm)	Depth		tie to	Hole, core, section, interval (cm)	Depth	
	(mbsf)	(mcd)			(mbsf)	(mcd)
1022B-1H-4, 95	5.45	5.45	tie to	1022A-2H-1, 51	5.01	5.45
1022A-2H-6, 31	12.31	12.75	tie to	1022C-2H-4, 75	12.75	12.75
1022C-2H-6, 99	15.99	15.99	tie to	1022A-3H-1, 83	14.83	15.99
1022A-3H-4, 55	19.05	20.21	tie to	1022C-3H-2, 115	19.65	20.21
1022C-3H-6, 23	24.73	25.29	tie to	1022A-4H-2, 18	25.18	25.29
1022A-4H-6, 71	31.71	31.82	tie to	1022C-4H-4, 83	31.83	31.82
1022C-4H-7, 13	35.63	35.62	tie to	1022A-5H-2, 103	35.53	35.62
1022A-5H-6, 51	41.01	41.1	tie to	1022B-5H-4, 1	39.21	41.10
1022B-5H-6, 127	43.47	45.36	tie to	1022A-6H-1, 103	43.53	45.36
1022A-6H-7, 7	51.57	53.4	tie to	1022B-6H-6, 11	51.81	53.4
1022B-6H-7, 43	53.63	55.22	tie to	1022A-7H-1, 67	52.67	55.22
1022A-7H-5, 11	58.11	60.66	tie to	1022C-7H-2, 83	57.33	60.66
1022C-7H-6, 118	63.68	67.01	tie to	1022A-8H-1, 75	62.25	67.01
1022A-8H-6, 127	70.27	75.03	tie to	1022C-8H-5, 13	70.63	75.03
1022C-8H-6, 138	73.38	77.78	tie to	1022A-9H-2, 31	72.81	77.78
1022A-9H-6, 67	79.17	84.14	tie to	1022C-9H-4, 118	79.68	84.14
1022C-9H-7, 23	83.23	87.69	tie to	1022A-10H-2, 115	83.15	87.69
1022A-10H-3, 119	84.69	89.23	tie to	1022C-10H-1, 108	84.58	89.23
1022C-10H-6, 88	91.88	96.53	tie to	1022A-11H-1, 107	91.07	96.53
1022A-11H-6, 127	98.77	104.23	tie to	1022C-11H-5, 13	99.13	104.23
1022C-11H-6, 123	101.73	106.83	tie to	1022A-12H-2, 31	101.35	106.83
1022A-12H-6, 139	108.43	113.91	tie to	1022C-12H-5, 28	108.78	113.91
1022C-12H-7, 43	111.93	117.06	tie to	1022A-13H-2, 71	111.21	117.06
1022A-13H-7, 19	118.19	124.04	tie to	1022C-13H-5, 38	118.41	124.04
1022C-13H-7, 23	121.26	126.89	tie to	1022A-14H-1, 87	119.37	126.89
1022A-14H-6, 59	126.59	134.11	tie to	1022C-14H-4, 98	126.98	134.11
1022C-14H-7, 38	130.88	138.01	tie to	1022A-15H-1, 59	128.59	138.01
1022A-15H-6, 27	135.77	145.19	tie to	1022C-15H-5, 68	137.68	145.19
1022C-15H-7, 8	140.08	147.59	tie to	1022A-16H-1, 39	137.89	147.59
1022A-16H-4, 55	142.55	152.25	tie to	1022C-16H-2, 23	142.23	152.25
1022C-16H-7, 73	150.26	160.28	tie to	1022A-17H-1, 34	147.34	160.28
1022A-17H-7, 79	156.79	169.73				

Note: This table is also on CD-ROM, back pocket, this volume.

Table 10. Interstitial water geochemical data, Hole 1022A.

Core, section, interval (cm)	Depth (mbsf)	pH	Alkalinity		Cl ⁻ (mM)	Na ⁺ (mM)	SO ₄ ²⁻ (mM)	HPO ₄ ²⁻ (μM)	NH ₄ ⁺ (mM)	H ₄ SiO ₄ (μM)	Ca ²⁺ (mM)	Mg ²⁺ (mM)	Sr ²⁺ (μM)	Li ⁺ (μM)	K ⁺ (mM)	
			(mM)	Salinity												
167-1022A-																
1H-2, 145-150	2.95	7.71	4.56	34.5	550	475	23.5	16	0.26	702	9.09	48.8	80	27	11.1	
2H-3, 145-150	8.95	7.93	7.03	34.0	553	476	17.9	37	0.57	846	8.11	46.5	89	27	10.5	
3H-3, 145-150	18.45	7.70	11.2	33.0	559	484	9.3	41	1.15	908	6.06	41.2	95	32	10.1	
4H-3, 145-150	27.95	7.58	14.4	33.0	560	488	3.3	79	1.58	1005	4.49	36.8	99	36	10.5	
5H-3, 145-150	37.45	7.50	16.4	33.0	561	490	<0.4	70	2.02	1001	4.12	34.4	111	43	10.2	
6H-3, 145-150	46.95	7.45	15.6	32.0	557	491	<0.4	69	2.49	1001	4.34	31.8	117	46	9.7	
9H-3, 145-150	75.45	7.60	15.1	32.0	556	495	<0.4	43	3.56	1020	4.63	29.0	142	64	9.1	
12H-3, 145-150	103.99	7.39	15.6	32.0	551	494	<0.4	16	4.50	831	4.98	26.8	157	93	9.0	
15H-3, 145-150	132.45	7.50	16.4	32.0	550	495	<0.4	12	5.21	975	5.94	25.2	169	131	8.7	
18H-2, 145-150	160.95	7.31	16.8	32.0	551	499	<0.4	8	5.67	992	6.43	23.4	182	167	8.7	

of the density-porosity combination tool string (pass 1: 390-98 mbsf; pass 2: 386-89 mbsf), two full passes of the sonic-FMS tool string (pass 1: 388-88 mbsf; pass 2: 388-85 mbsf), and two passes of the GHMT tool string (pass 1: 388-78 mbsf; pass 2: 383-65 mbsf) were conducted. The NRMT (total magnetic moment) cartridge of the GHMT tool string was not operational at this hole (or any of the other holes logged during Leg 167), but the SUMT cartridge, which measures magnetic susceptibility, was fully operational. Sea-state conditions were rough (3- to 4-m swells), and the wireline heave compensator was used on all passes.

Borehole caliper measurements conducted during the density-porosity combination and sonic-FMS tool runs indicate that the borehole was significantly washed out (diameter >14 in) above 160 mbsf, a level that roughly corresponds to the APC/XCB coring transition. Regularly spaced 10-m washouts between 250 and 300 mbsf can be attributed to circulation during XCB drilling (Fig. 18). Overall log quality at this site is very good over most of the logged interval.

The TLT was run during both passes of the density-porosity combination tool. The temperature logs were linked to the actual logging depths using the time-depth log recorded at the logging unit. The raw

TLT results show a minimum downhole thermal gradient of 23°C/km (Fig. 19); this is, however, an underestimate because of the cooling effects of seawater circulation. In situ temperature measurements using the Adara probe indicate a thermal gradient near 88°C/km at this site (see “Physical Properties” section, this chapter).

Lithology

Physical properties changes measured by the logs are associated with the broad lithostratigraphic shifts at Site 1022. The transition from chert and porcellanite to clayey diatom ooze associated with the Subunit IIIA/Subunit IIIB boundary (360 mbsf) is indicated by a marked increase in density and a reduction in porosity downhole. Similarly, the transition from clayey diatom ooze to more clay-rich lithologies associated with the Subunit IIB/Subunit IIIA boundary near 240 mbsf occurs as a gradual shift toward lower density and higher porosity values, with characteristically higher gamma-ray values downhole. Numerous dolostone stringers are detected in the FMS images. These stringers occur as thin, discrete beds (~10-60-cm thick) near 166, 172, 204, 210, 216, 338, and 341 mbsf. Numerous

Table 11. Interstitial water geochemical data, Hole 1022C.

Core, section, interval (cm)	Depth (mbsf)	pH	Alkalinity (mM)	Salinity
167-1022C-				
21X-3, 145–150	188.85	7.20	16.41	31.5
24X-3, 145–150	217.65	7.35	16.21	31.8
27X-3, 145–150	246.55	7.34	17.60	32.0
30X-3, 145–150	275.45	7.34	16.10	31.5
33X-3, 145–150	304.35	7.20	15.48	31.8
36X-3, 140–150	333.30	7.13	14.95	32.0
39X-3, 140–150	362.20	7.25	14.55	32.0

thin (5–15 cm), highly resistive (chert?) beds occur between 370 and 384 mbsf in association with lithostratigraphic Subunit IIIB.

SUMMARY

Site 1022, part of the Gorda Transect, was the last site drilled on Leg 167 and, because the final transit to port in San Francisco was short, most of the available information is from Hole 1022A (drilled to 166 mbsf), including shipboard age control (Fig. 20). All age dating deeper than 166 mbsf is speculative. Site 1022 was triple cored from 0–101 mbsf (~2.3–3.3 Ma), double cored to 166 mbsf (~3.6 Ma), and a single hole was drilled to 388 mbsf. Drilling objectives for Site 1022 were to recover a Neogene sediment column from the lower slope of the California Margin. Instead, we drilled a high-resolution Pliocene to possibly upper Miocene interval, assuming the average sedimentation rate above 166 mbsf is representative for the sediments below and assuming that the silica-rich sediments are most

probably Miocene in age. The top of the sediment column is a hiatus, with roughly a meter of Pleistocene sediments over upper Pliocene sediments older than ~2.3 Ma. The Pliocene sediments are unconsolidated and resemble Pleistocene sediments at other Leg 167 sites in terms of their physical properties. Because the sediments have never been deeply buried, it is clear that the hiatus is not an erosional event or an unconformity left by a slump but probably represents a long period when no sediments were deposited.

REFERENCES

- Bordovskiy, O.K., 1965. Accumulation and transformation of organic substances in marine sediment, 2. Sources of organic matter in marine basins. *Mar. Geol.*, 3:5–31.
- Emerson, S., and Hedges, J.I., 1988. Processes controlling the organic carbon content of open ocean sediments. *Paleoceanography*, 3:621–634.
- Ingle, J.C., Jr., 1973. Summary comments on Neogene biostratigraphy, physical stratigraphy, and paleo-oceanography in the marginal northeastern Pacific Ocean. In Kulm, L.D., von Huene, R., et al., *Init. Repts. DSDP*, 18: Washington (U.S. Govt. Printing Office), 949–960.
- Lyle, M., Gallaway, P.J., Liberty, L.M., Mix, A., Stott, L., Hammond, D., Gardner, J., Dean, W., and the EW9504 Scientific Party, 1995a. Data submission. W9406 and EW9504 site surveys of the California margin proposed drillsites, Leg 167 (Vol. 1): Site maps and descriptions. Boise State Univ., *CGISS Tech. Rep.*, 95–11.
- _____, 1995b. Data submission. W9406 and EW9504 site surveys of the California margin proposed drillsites, Leg 167 (Vol. 2): Seismic profiles. Boise State Univ., *CGISS Tech. Rep.*, 95–12.

Ms 167IR-116

NOTE: For all sites drilled, core-description forms (“barrel sheets”) and core photographs can be found in Section 3, beginning on page 499. Smear-slide data can be found in Section 4, beginning on page 1327. See Table of Contents for material contained on CD-ROM.

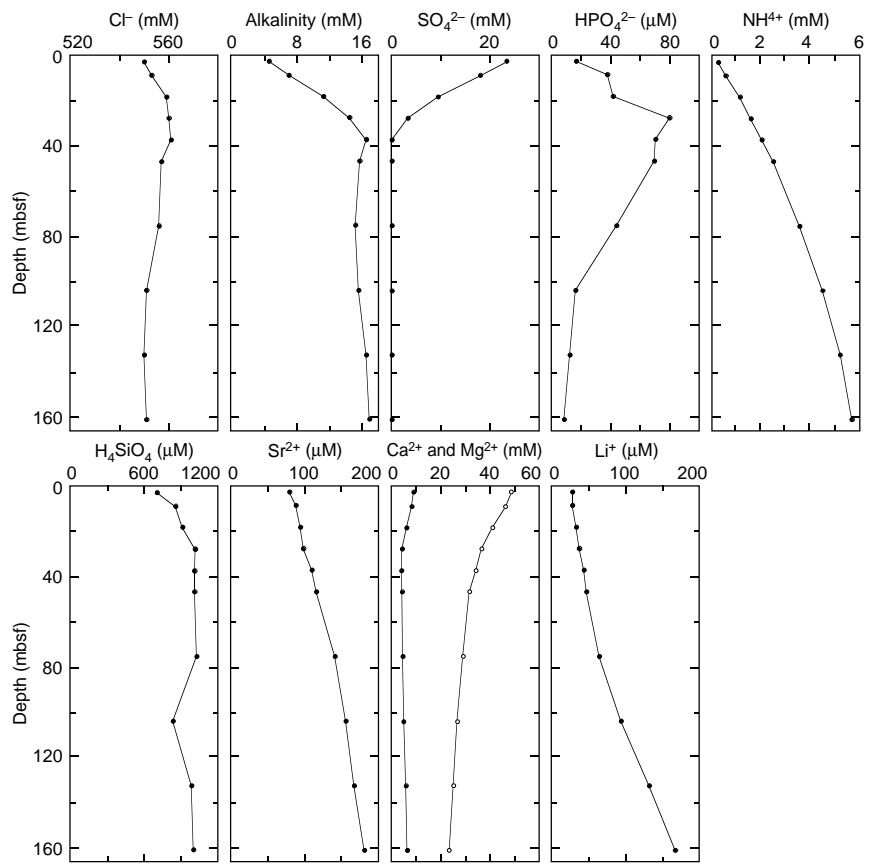


Figure 9. Interstitial water geochemical data, Site 1022. Solid circles = Ca, open circles = Mg.

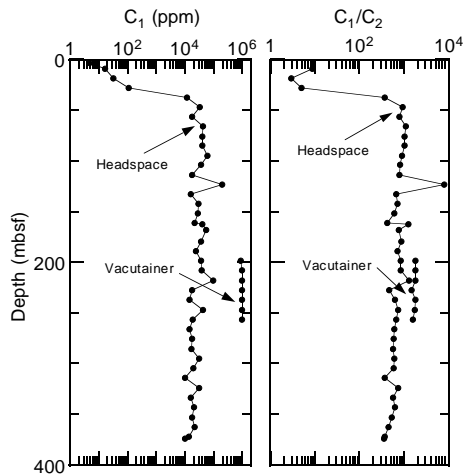


Figure 10. Depth variations of methane (C₁) concentration and methane/ethane (C₁/C₂) ratios obtained by the headspace and vacutainer techniques from Hole 1022A.

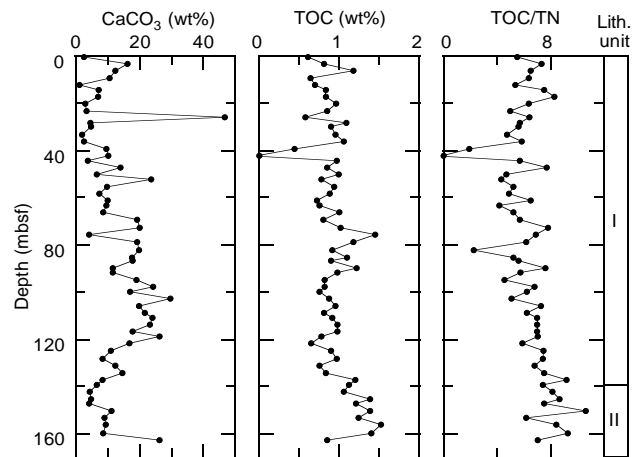


Figure 11. Depth variations of calcium carbonate, total organic carbon (TOC), and total organic carbon/total nitrogen (TOC/TN) ratios in sediments of Hole 1022A.

Table 12. Concentrations of methane (C₁), ethene (C₂₌), ethane (C₂), propene (C₃₌), propane (C₃), isobutane (i-C₄), n-butane (n-C₄), isopentane (i-C₅), n-pentane (n-C₅), isohexane (i-C₆) and n-hexane (n-C₆) obtained by the headspace (Holes 1022A and 1022C) and vacutainer techniques (Hole 1022C).

Core, section, interval (cm)	Depth (mbsf)	C ₁ (ppm)	C ₂₌ (ppm)	C ₂ (ppm)	C ₃₌ (ppm)	C ₃ (ppm)	i-C ₄ (ppm)	n-C ₄ (ppm)	i-C ₅ (ppm)	n-C ₅ (ppm)	i-C ₆ (ppm)	n-C ₆ (ppm)	C ₁ /C ₂
Headspace													
167-1022A-													
1H-3, 0-5	3.03	5											
2H-4, 0-5	9.03	17		2									9
3H-4, 0-5	18.53	33		11		7							3
4H-4, 0-5	28.03	117		23		15							5
5H-4, 0-5	37.53	11,753		32		19							367
6H-4, 0-5	47.03	33,521		36		14							931
7H-4, 0-5	56.53	18,381		23		12							799
8H-4, 0-5	66.03	44,811		40		18							1,120
9H-4, 0-5	75.53	40,977	7	40	3	25							1,024
10H-4, 0-5	85.03	41,513	2	40	3	30							1,038
11H-4, 0-5	94.53	61,493	3	68		51							904
12H-4, 0-5	104.03	36,731	2	45		36							816
13H-4, 0-5	113.53	18,380		23		12	19	14	13	16	10	5	799
14H-4, 0-5	123.03	209,121	1	26		20	18	12	11	15			8,043
15H-4, 0-5	132.53	15,969	2	24	3	24	19	16	13	17	10	4	665
16H-4, 0-5	142.03	31,279	1	43		34	21	14	14	16	10	4	727
17H-4, 0-5	151.53	28,524	7	46		38	21	14	13	15	10	4	620
18H-4, 0-5	161.03	23,028	3	54	3	66	22	15	14	16	5		426
167-1022C													
18X-3, 0-5	162.53	40,919		33		10	19	13	12	15	10	4	1,240
19X-3, 0-5	168.23	56,072	2	72		61	26	15	14	16	10	4	779
20X-4, 0-5	179.33	36,777		42		29	22	14	12	15	10	4	876
21X-4, 0-5	188.93	24,973	1	35		35	22	15	11	15	10	4	714
22X-4, 0-5	198.53	36,931	7	43		35	21	13	11	15			859
23X-4, 0-5	208.13	38,781		46		43	26	15	13	15	10		843
24X-4, 0-5	217.73	96,258	1	73		50	22	14	12	15			1,319
25X-4, 0-5	227.43	18,031	1	38		45	25	15	14	15	10		475
26X-4, 0-5	237.03	14,581		23		23	25	15	14	15	10		634
27X-4, 0-5	246.63	44,935	8	60		54	24	15	14	16	10	4	749
28X-4, 0-5	256.33	19,079		28		25	27	16	14	16	10	4	681
29X-4, 0-5	265.93	14,725		24		27	24	14	14	16	10	5	614
30X-4, 0-5	275.53	18,000		30		31	20	13	12	15	10		600
31X-4, 0-5	285.13	17,189	1	30		36	22	14	13	15	10		573
32X-4, 0-5	294.83	32,291	1	53		58	29	17	16	15	11	5	609
33X-4, 0-5	304.43	19,898	1	34		39	28	17	16	15	11	5	585
34X-4, 0-5	314.13	10,591	2	29		42	28	17	17	15	11	5	365
35X-4, 0-5	323.83	32,515	1	43		39	23	15	14	15	10		756
36X-4, 0-5	333.43	16,848	1	29		34	18	19	19	15	11	4	581
37X-4, 0-5	343.13	21,578		34		34	26	17	17	16	16	10	635
38X-5, 0-5	367.73	18,670		35		37	21	15	14	15			533
39X-4, 0-5	362.33	22,471	1	50		62	37	24	28	19	13	5	449
40X-3, 0-5	370.43	14,273		39		42	27	18	20	17	12	5	366
41X-1, 0-5	374.03	10,474	1	29		30	26	18	26	18	20	18	361
Vacutainer													
167-1022-C													
22X-4, 0-5	198.53	901,439		504		129	26	14	11	15			1,789
23X-4, 0-5	208.13	1,011,160		561		159	32	14	12	17			1,802
24X-4, 0-5	217.73	995,776		550		153	37	15	12	19			1,811
25X-4, 0-5	227.43	969,873		653		210	39	16	13	15			1,485
26X-4, 0-5	237.03	1,018,120		560		163	28	14	12	15			1,818
27X-4, 0-5	246.63	994,856		574		167	23	13	11	17	10	4	1,733
28X-4, 0-5	256.33	1,012,900		626		191	33	15	12	15			1,618

Table 13. Concentrations of inorganic carbon, calcium carbonate, total carbon, total organic carbon, total nitrogen, and total sulfur in weight percent (wt%) in Hole 1022A.

Core, section, interval (cm)	Depth (mbsf)	Inorganic carbon (wt%)	CaCO ₃ (wt%)	Total carbon (wt%)	Total organic carbon (wt%)	Total nitrogen (wt%)	Total sulfur (wt%)	Total organic carbon/Total nitrogen
167-1022A-								
1H-1, 58-59	0.58	0.32	2.67	0.93	0.61	0.11	0.12	5.55
1H-3, 28-29	3.29	1.96	16.33	2.77	0.81	0.11	0.16	7.36
2H-2, 29-30	6.29	1.51	12.58	2.69	1.18	0.18	0.28	6.56
2H-4, 29-30	9.29	1.29	10.75	1.93	0.64	0.1	0.13	6.4
2H-6, 29-30	12.29	0.16	1.33	0.86	0.7	0.13	0.18	5.38
3H-1, 29-30	14.29	0.87	7.25	1.7	0.83	0.11	0.24	7.55
3H-3, 29-30	17.29	0.86	7.16	1.69	0.83	0.1	0.21	8.3
3H-5, 29-30	20.29	0.37	3.08	1.33	0.96	0.15	0.45	6.4
3H-7, 29-30	23.29	0.41	3.42	1.26	0.85	0.17	0.32	5
4H-2, 89-90	25.89	5.62	46.81	6.2	0.58	0.09	0.11	6.44

Only part of this table is produced here. The entire table appears on CD-ROM (back pocket).

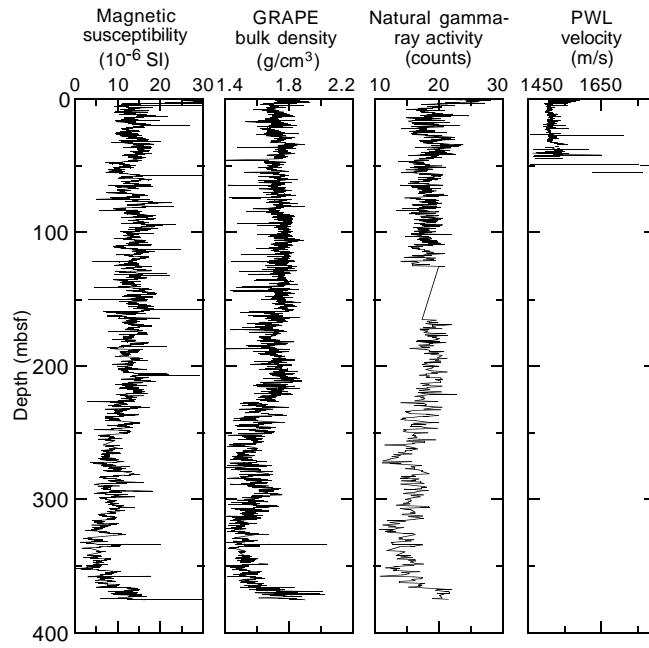


Figure 12. MST data from Hole 1022A.

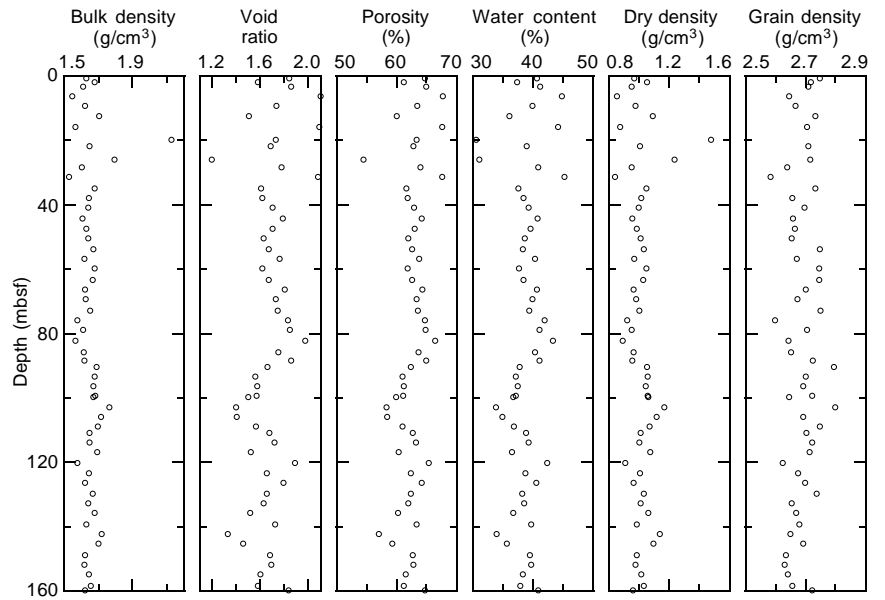


Figure 13. Index property data from Hole 1022A.

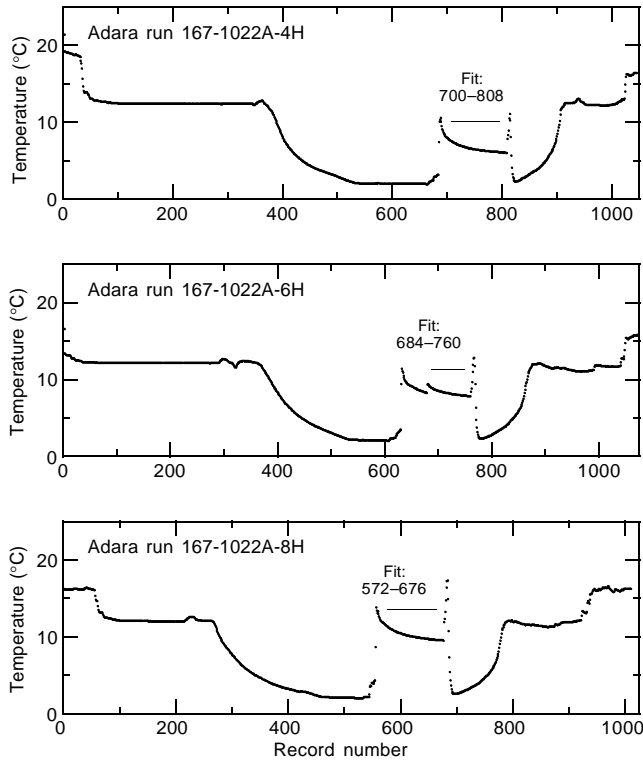


Figure 14. Hole 1022A downhole temperature vs. record number (5-s recording frequency) for each measurement run, showing the intervals fitted to determine the downhole temperature.

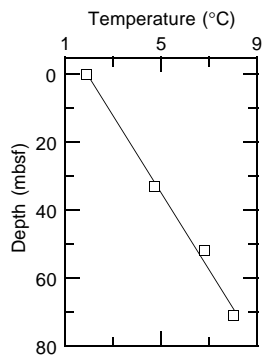


Figure 15. Downhole temperature gradient for Hole 1022A.

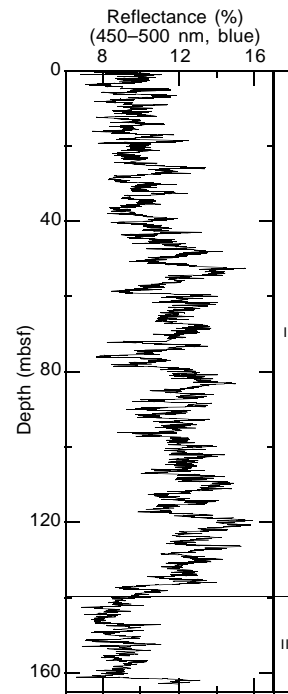


Figure 16. Percent color reflectance for the 450–500-nm band average (blue) shown with lithostratigraphic units from Hole 1022A.

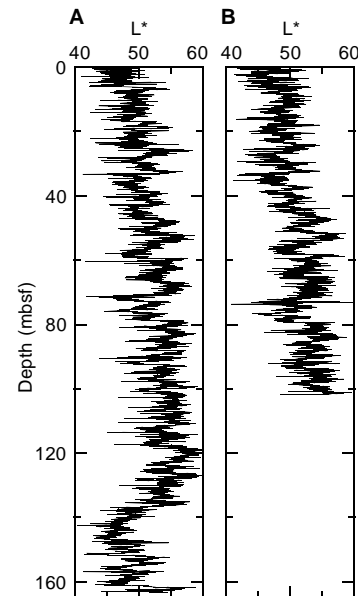


Figure 17. Intensity of color CIELAB L* from the digital color video data from (A) Holes 1022A and (B) 1022B. Data were decimated to 2-cm spacing.

Table 17. Downhole measurements in Hole 1022C.

Date, time	Description
14 June 1996	
1130	Set pipe at 80 mbsf, rig up wireline, rig up density-porosity combination tool string, seas rough (3- to 5-m swells).
1350	At TD, begin density-porosity pass 1 at 300 m/hr (390–98 mbsf).
1515	At TD, begin density-porosity pass 2 (386–89 mbsf), continue logging to mudline.
1700	POOH, rig down density-porosity, rig up sonic-FMS tool string, RIH.
1915	At TD, begin sonic-FMS pass 1 at 300 m/hr (388–88 mbsf).
2045	At TD, begin sonic-FMS pass 2 (388–85 mbsf).
2300	POOH sonic-FMS, rig down, rig up GHMT tool string, RIH.
15 June 1996	
0110	At TD, begin GHMT pass 1 at 1000 m/hr (388–78 mbsf).
0150	At TD, begin GHMT pass 2 (383–65 mbsf).
0330	POOH GHMT, rig down, end logging operations.

Note: RIH = run in hole, TD = total depth, FMS = formation microscanner, POOH = pull out of hole, GHMT = geological high-sensitivity magnetic tool.

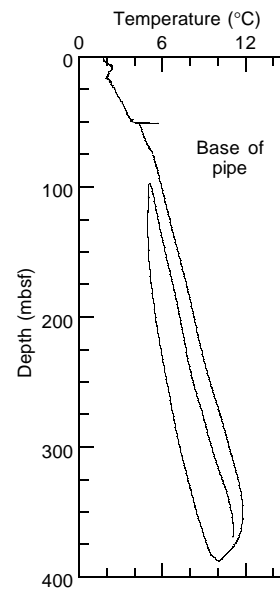


Figure 19. Borehole temperature measurements from the Lamont-Doherty temperature logging tool.

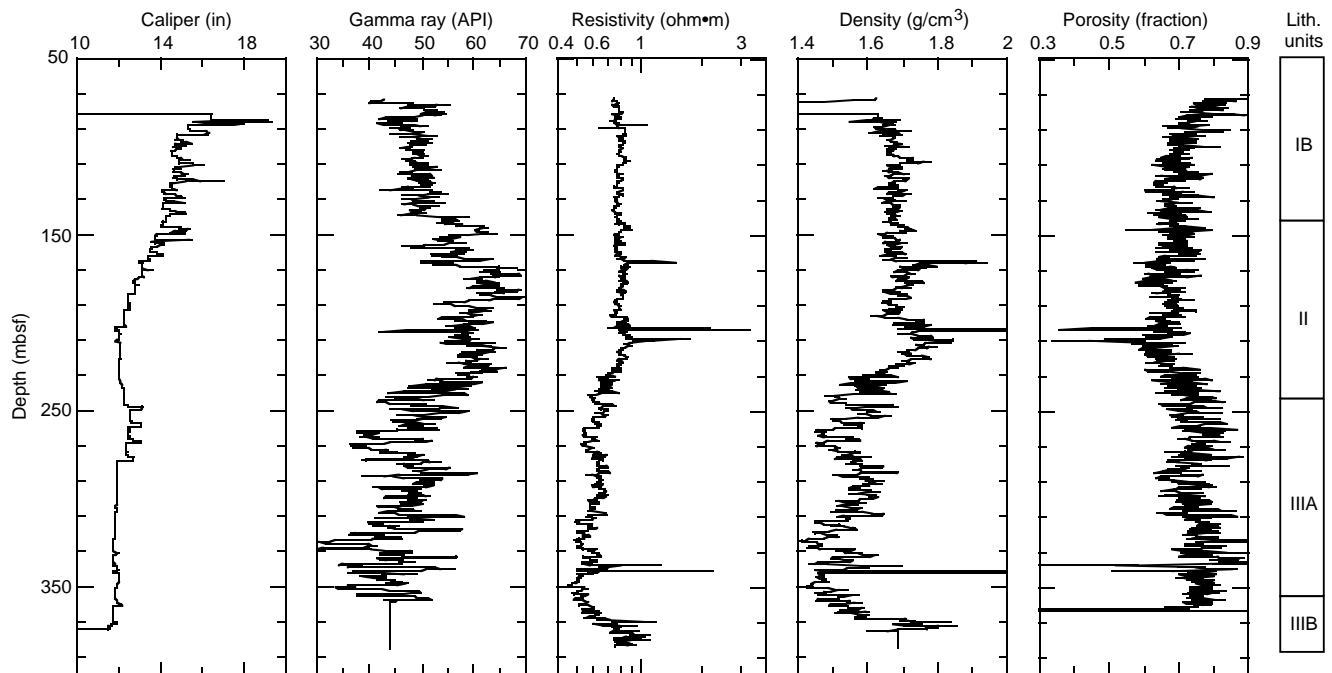


Figure 18. Downhole log data from the density-porosity combination tool string (pass 2) and a lithostratigraphic summary column of Hole 1022C (see “Lithostratigraphy” section, this chapter).

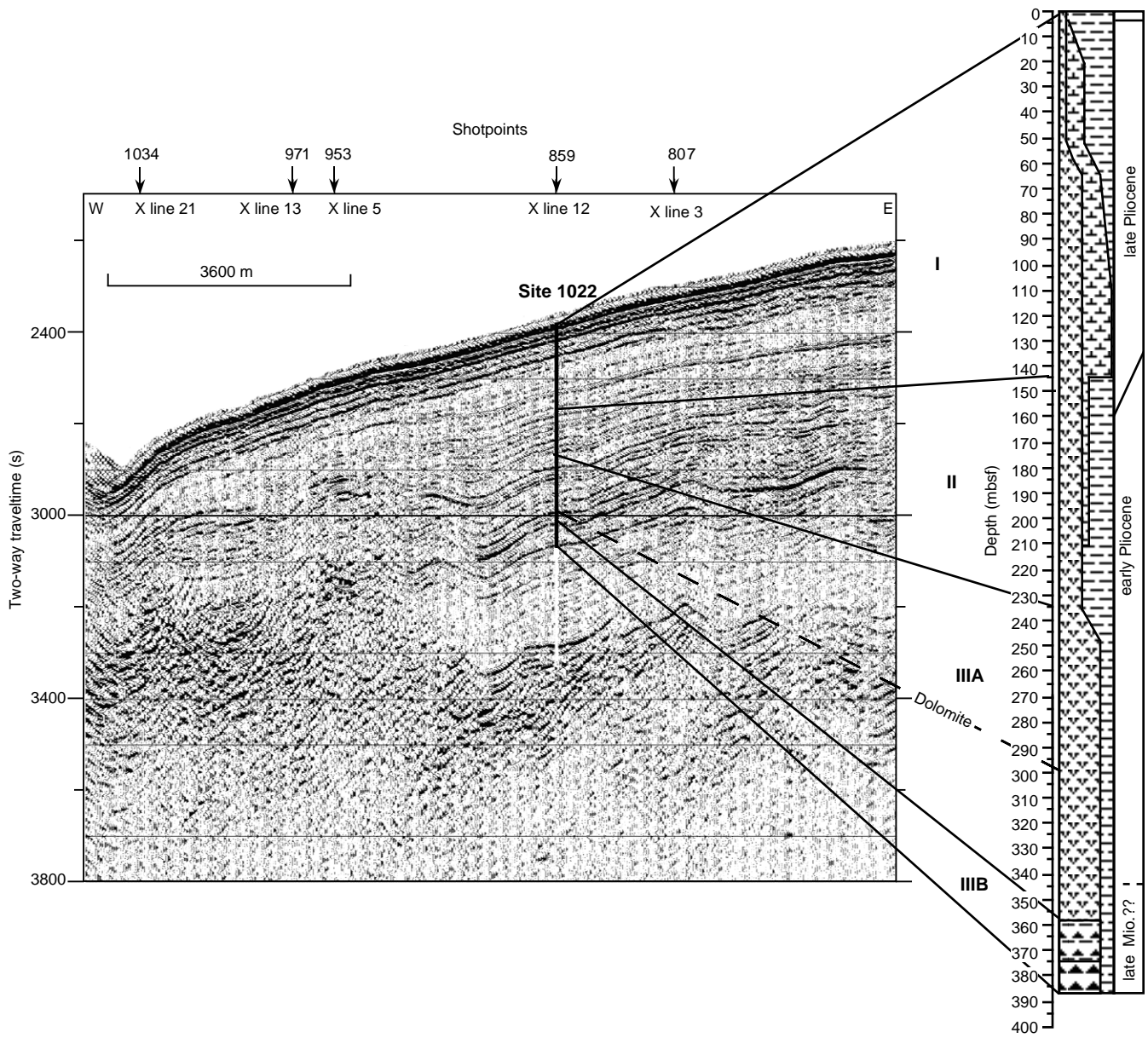


Figure 20. Comparison of the lithostratigraphic column at Site 1022 and a seismic reflection profile through it (Line EW9504 CA2-23; Lyle et al., 1995a, 1995b). Ties are calculated from shipboard seismic velocity measurements (see “Physical Properties” section, this chapter). On y-axis, (s) = milliseconds.

SHORE-BASED LOG PROCESSING HOLE 1022C

Bottom felt: 1937.5 mbrf (used for depth shift to seafloor)

Total penetration: 387.7 mbsf

Total core recovered: 378.8 m (97.7%)

Logging Runs

Logging string 1: DIT/HLDT/APS/SDT/HNGS (2 passes)

Logging string 2: FMS/GPIT/SDT/NGT (2 passes)

Logging string 3: GHMT/NGT (2 passes)

Wireline heave compensator was used to counter ship heave resulting from the rough sea conditions.

Bottom-Hole Assembly

The following bottom-hole assembly depths are as they appear on the logs after differential depth shift (see "Depth shift" section) and depth shift to the seafloor. As such, there might be a discrepancy with the original depths given by the drillers on board ship. Possible reasons for depth discrepancies are ship heave, use of wireline heave compensator, and drill string and/or wireline stretch.

DIT/S/HLDT/APS/HNGS: Recorded open-hole (pass 1).

DIT/S/HLDT/APS/HNGS: Bottom-hole assembly at ~52.5 mbsf (pass 2).

FMS/GPIT/NGT: Recorded open-hole (pass 1).

FMS/GPIT/NGT: Bottom-hole assembly at ~52.5 mbsf (pass 2).

GHMT/NGT: Recorded open-hole (pass 1).

GHMT/NGT: Bottom-hole assembly at ~52.5 mbsf (pass 2).

Processing

Depth shift: Original logs have been interactively depth shifted with reference to HNGS from DIT/S/HLDT/APS/HNGS pass 2, and to the seafloor (-1937.5 m). The program used is an interactive, graphical depth-match program which allows us to visually correlate logs and to define appropriate shifts.

Gamma-ray and environmental corrections: Corrections for borehole size and type of drilling fluid were performed on the NGT

data from the FMS/GPIT/SDT/NGT and GHMT/NGT tool strings. HNGS data from the DIT/HLDT/APS/HNGS tool string were corrected in real-time during the recording.

Acoustic data processing: The array sonic tool was operated in standard depth-derived borehole compensated mode, including long-spacing (8-10-10-12 ft) and short spacing (3-5-5-7 ft) logs. Because the original delay times from both passes are far higher than typical seawater values and are also affected by cycle skips, an attempt has been made using the best long-spacing set of transit times to eliminate some of the cycle skipping experienced during the recording. The results, however, are of very poor quality, because of the difficulty in editing the single transit times. The short-spacing configuration DTL (long-spacing delay time) from both pass 1 and 2, however, displays a decent correlation with the resistivity data and has been selected to derive the velocity profile at this hole. Because the velocity values are lower than the velocity of sea water, the data should be used qualitatively only.

Quality Control

Data recorded through bottom-hole assembly should be used qualitatively only because of the attenuation on the incoming signal.

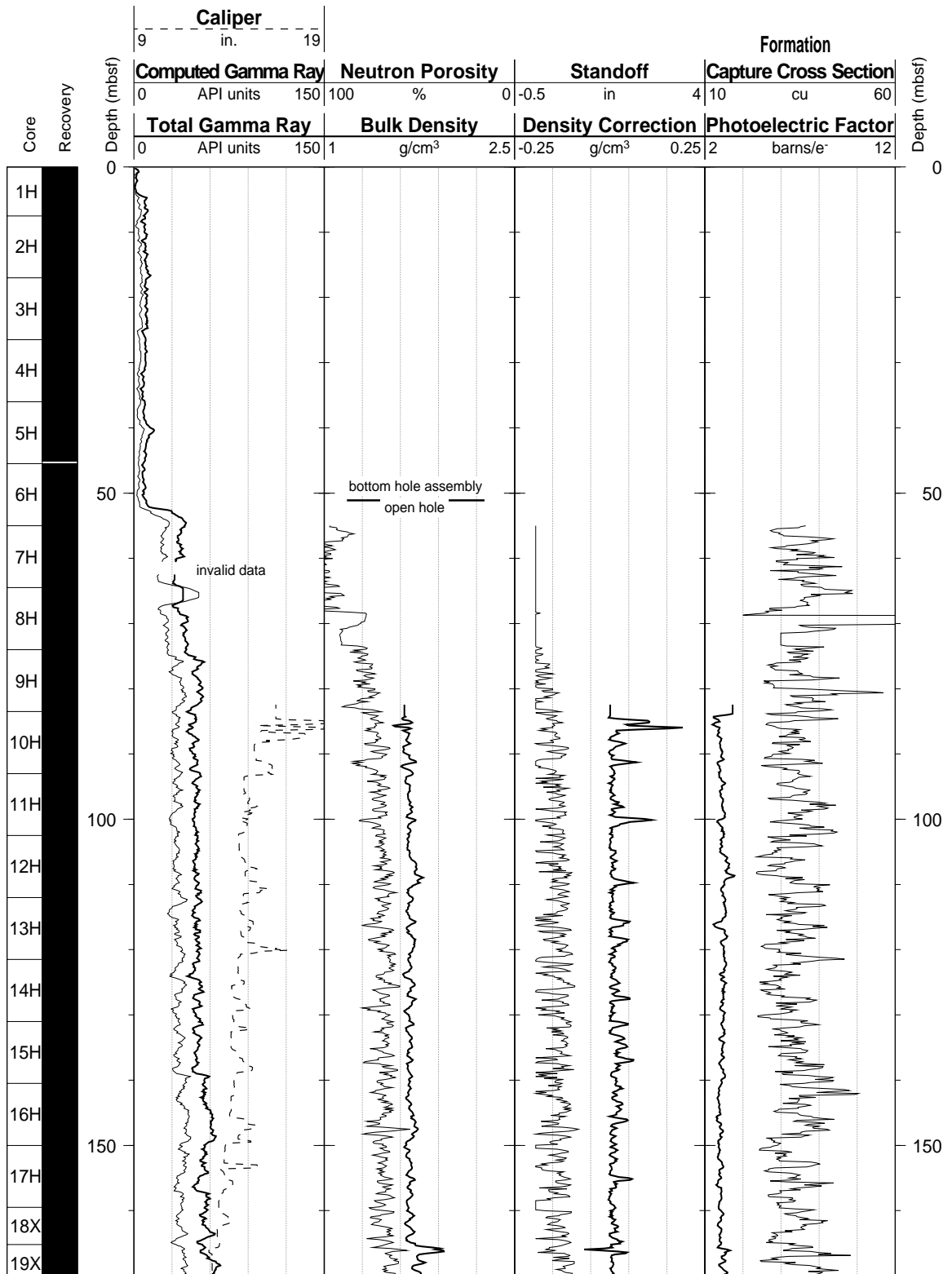
Hole diameter was recorded by the hydraulic caliper on the HLDT tool (CALI) and on the FMS string (C1 and C2). No good caliper measurements were recorded during FMS pass 1.

Note: Details of standard shore-based processing procedures are found in the "Explanatory Notes" chapter, this volume. For further information about the logs, please contact:

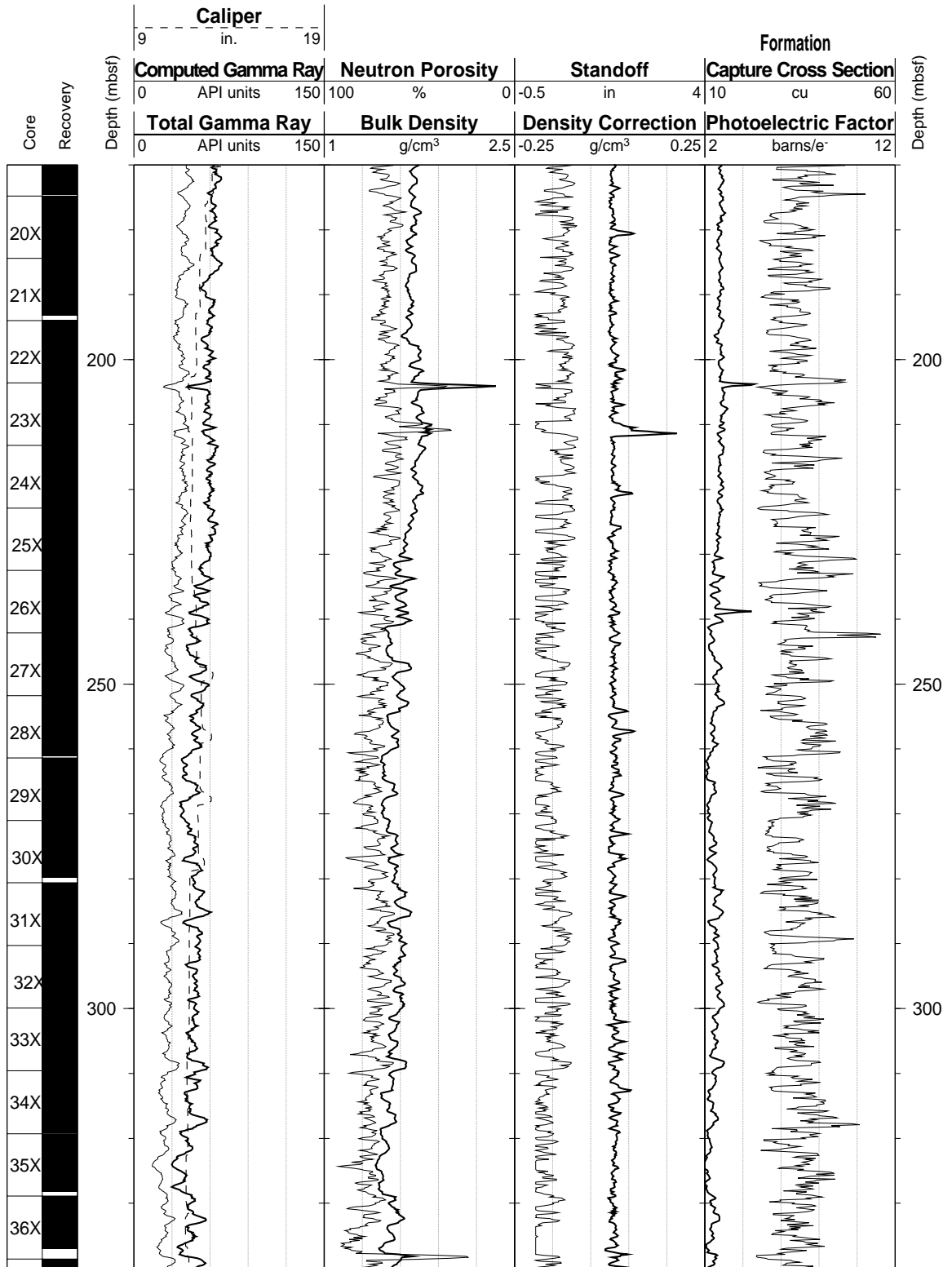
Cristina Broglia
Phone: 914-365-8343
Fax: 914-365-3182
E-mail: chris@ldeo.columbia.edu

Amal Chakraborty
Phone: 914-365-8358
Fax: 914-365-3182
E-mail: amalc@ldeo.columbia.edu

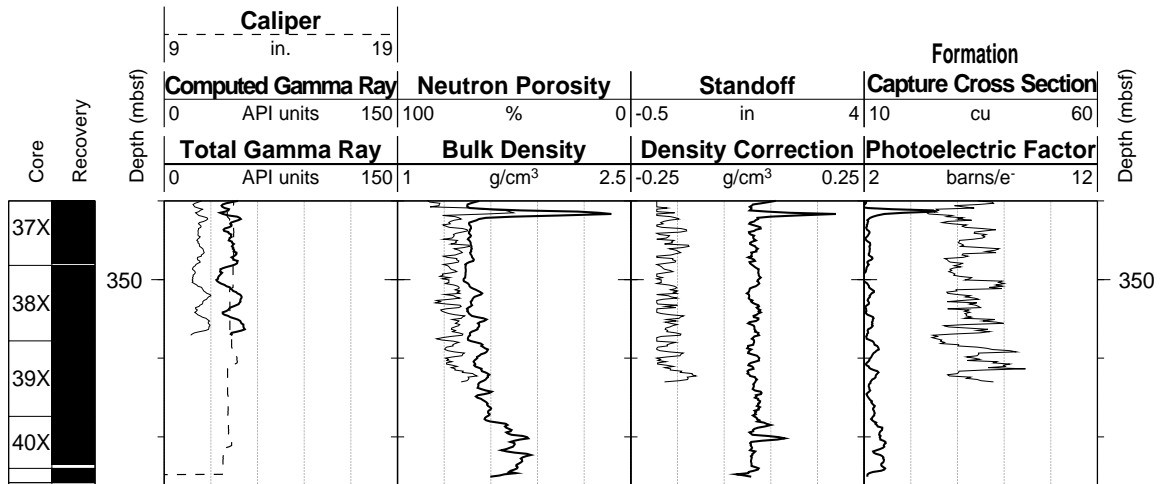
Hole 1022C: Natural Gamma Ray-Density-Porosity Logging Data-Pass 2



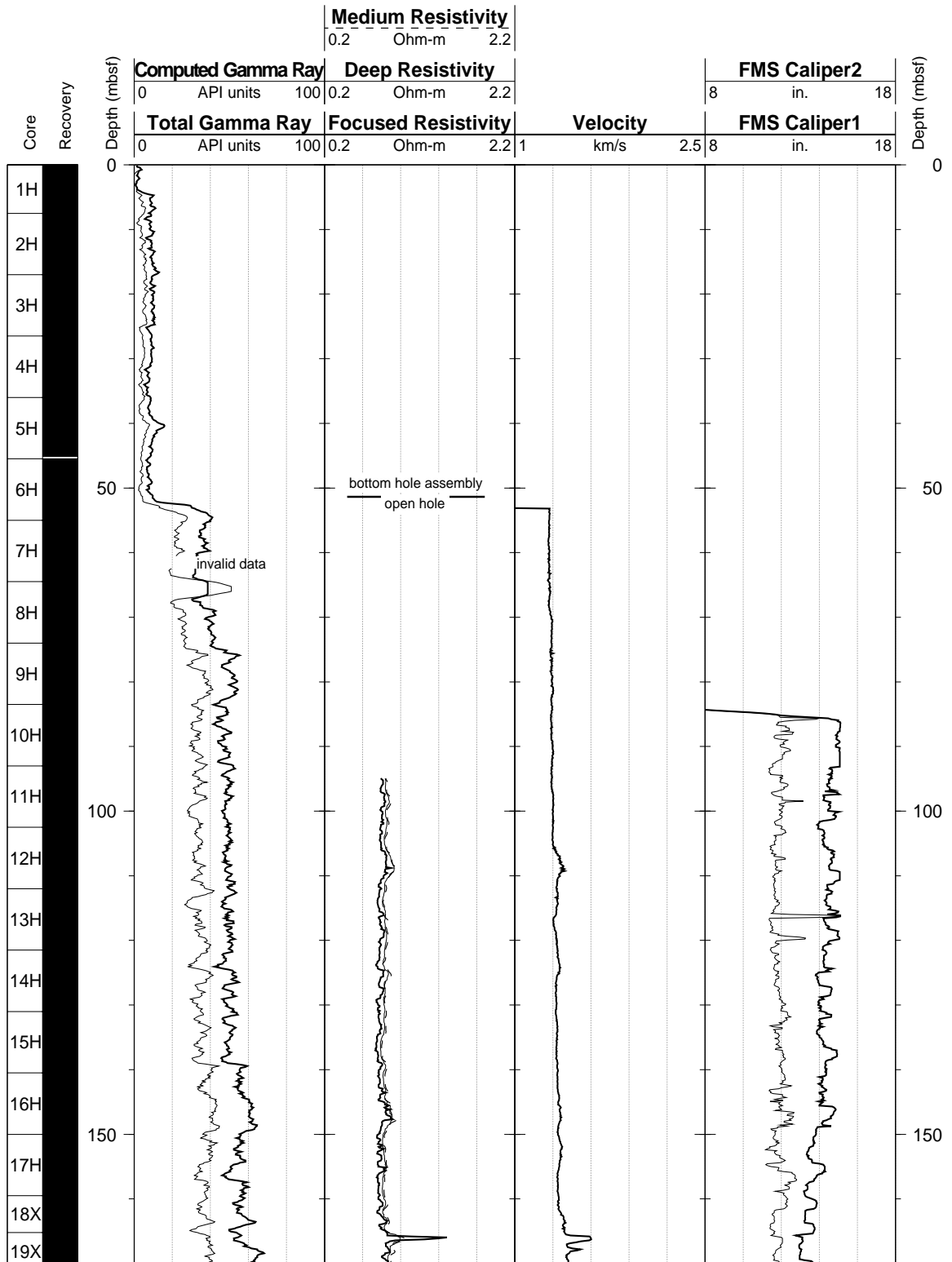
Hole 1022C: Natural Gamma Ray-Density-Porosity Logging Data-Pass 2 (cont.)



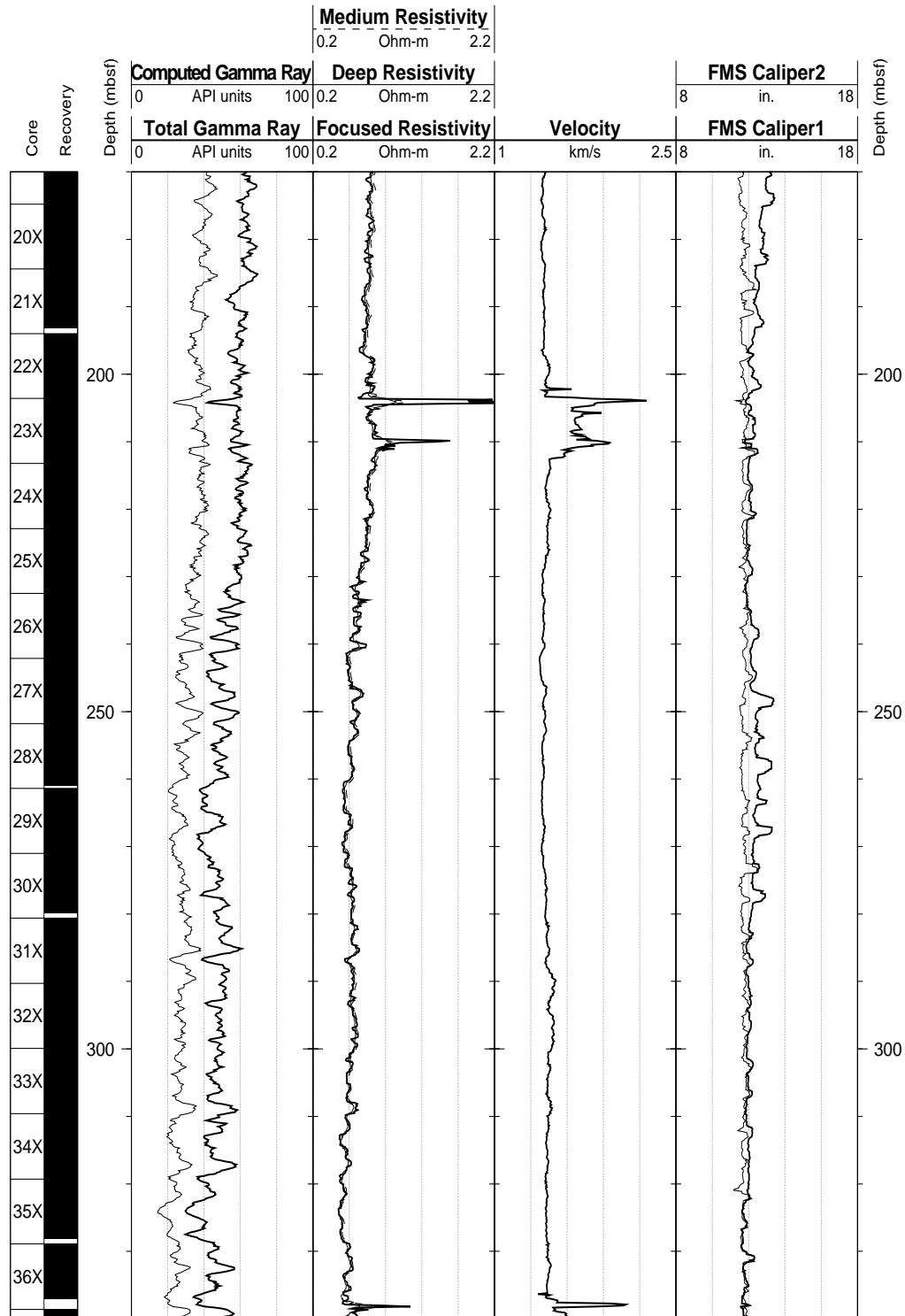
Hole 1022C: Natural Gamma Ray-Density-Porosity Logging Data-Pass 2 (cont.)



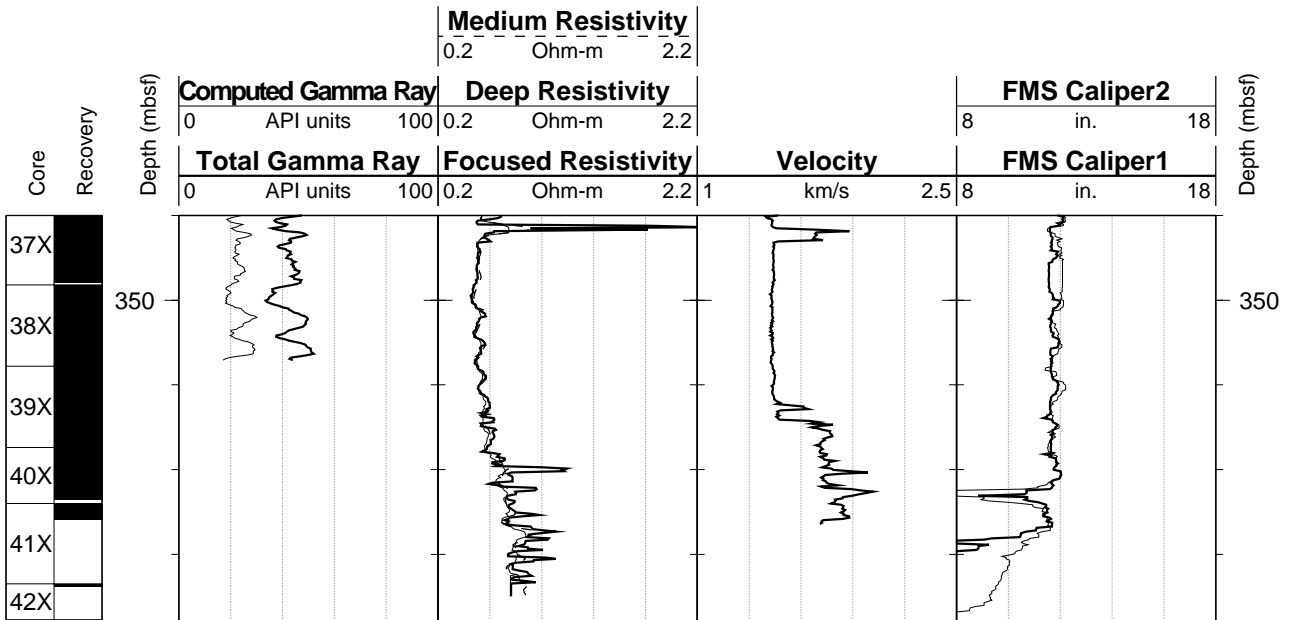
Hole 1022C: Natural Gamma Ray-Resistivity-Sonic Logging Data-Pass 2



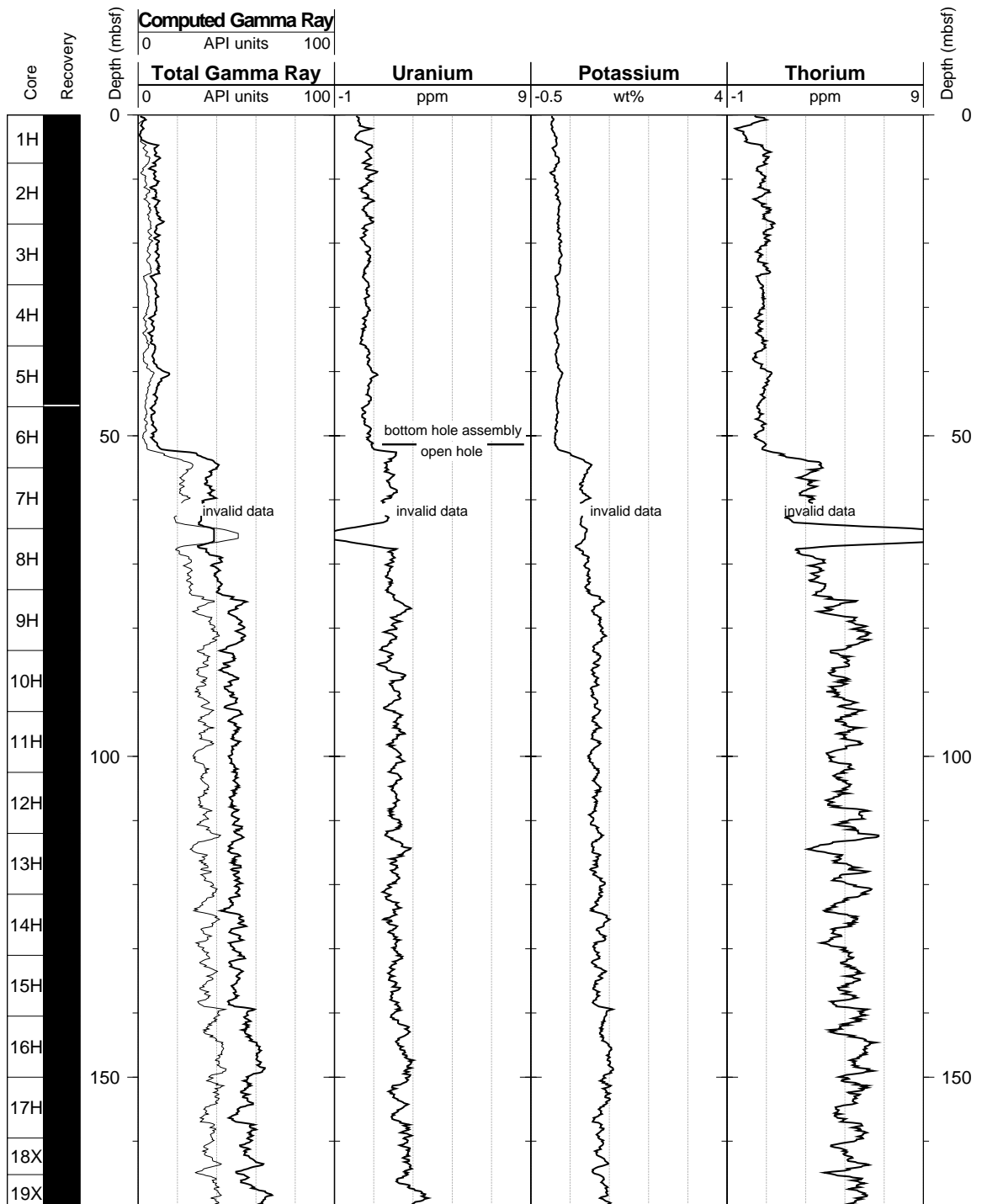
Hole 1022C: Natural Gamma Ray-Resistivity-Sonic Logging Data-Pass 2 (cont.)



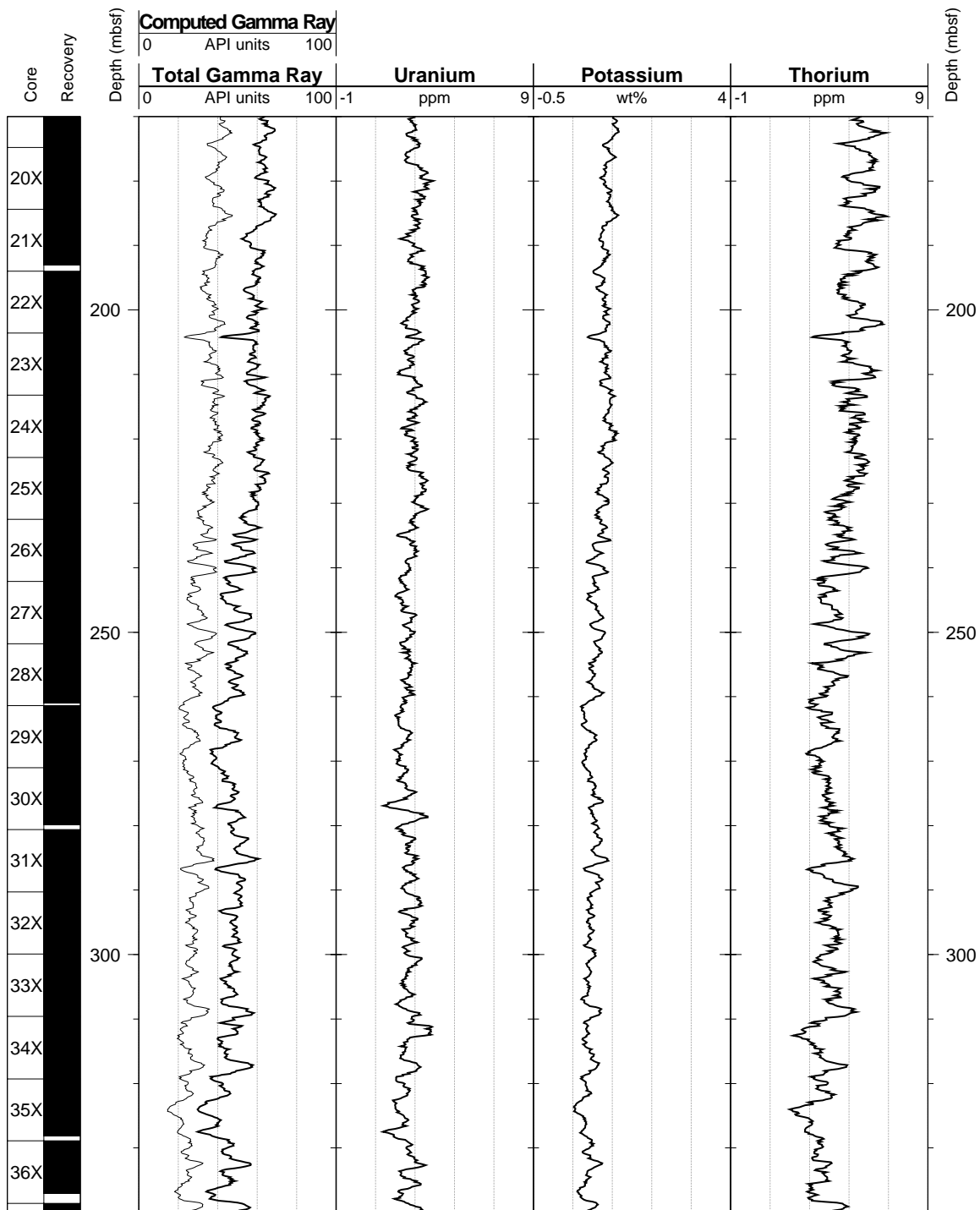
Hole 1022C: Natural Gamma Ray-Resistivity-Sonic Logging Data-Pass 2 (cont.)



Hole 1022C: Natural Gamma Ray Logging Data-Pass 2



Hole 1022C: Natural Gamma Ray Logging Data-Pass 2 (cont.)



Hole 1022C: Natural Gamma Ray Logging Data-Pass 2 (cont.)

